

**Climate changes during the Early–Middle Triassic transition in the E. Iberian plate and their palaeogeographic significance in the western Tethys continental domain**

Violeta Borrueal-Abadía<sup>a</sup>, José López-Gómez<sup>a\*</sup>, Raúl De la Horra<sup>b</sup>, Belén Galán-Aballán<sup>b</sup>, José F. Barrenechea<sup>a,c</sup>, Alfredo Arche<sup>a</sup>, Ausonio Ronchi<sup>d</sup>, Nicola Gretter<sup>d</sup>, Mariano Marzo<sup>e</sup>

<sup>a</sup> Instituto de Geociencias (CSIC, UCM), C/José Antonio Nováis 12, 28040 Madrid, Spain.

<sup>b</sup> Dept. of Stratigraphy, Faculty of Geology, Universidad Complutense de Madrid, 28040 Madrid, Spain.

<sup>c</sup> Dept. of Crystallography and Mineralogy, Faculty of Geology, Universidad Complutense de Madrid, 28040 Madrid, Spain.

<sup>d</sup> Dept. of Earth and Environmental Sciences, University of Pavia, Via Ferrata 1, 27100 Pavia, Italy.

<sup>e</sup> Dept. of Stratigraphy, Palaeontology and Marine Geosciences, Faculty of Geology, Universitat de Barcelona, 08028 Barcelona, Spain.

\* Corresponding author: Instituto de Geociencias (CSIC, UCM), C/José Antonio Novais 12, 28040 Madrid, Spain. Fax: +34 91 39444808, Telephone: + 34 91 3944783, E-mail: [jlopez@geo.ucm.es](mailto:jlopez@geo.ucm.es) (J. López-Gómez)

**Abstract**

Until recently the climate of the Early–Middle Triassic at low latitudes was broadly considered as generally temperate-warm with no major climate oscillations. This work examines the climate of this period through a detailed study of the sedimentary, plant, soil and mineral records of continental rocks (Buntsandstein facies) in eastern Iberian basins. Our findings indicate temporal climate variations for these near equator (10°–14°N) regions and unveil the significance of such variations in the southern Laurasian domain.

The climate of Iberia's Early Triassic was mainly dominated by alternating brief ( $< 0.4$  ma) arid and semi-arid climate periods, with two main arid periods documented at the end of the Smithian and middle Spathian. However, an initial short subhumid to semi-arid period was also observed in the late Spathian. Remarkably, this latter period appears just after an unconformity related to the tectonically induced Hardegsen Event in western Europe. It is also of interest that this short subhumid climate period is concurrent with the beginning of faunal and floral recovery in the basins examined. The Early Triassic ended again with a short very arid period.

Although the beginning of the Anisian (Aegean) was represented by alternating arid and semi-arid to subhumid intervals, during the Bithynian and Pelsonian clearly wetter climates are recorded by the succession consisting of alternating semi-arid to semi-humid intervals. This general tendency was interrupted by three short but marked intervals, two humid intervals in the late Bithynian, and one arid period near the Bithynian/Pelsonian boundary.

Iberia was crossed by prominent irregular highs separating marked corridors or isolated areas. This palaeogeography, prevailing since Variscan tectonics, clearly conditioned dominant climates and their geographical distribution. No clear climate belts developed in these conditions. However, isolated internal climate zones separated by elevated areas are identified. This palaeogeographic configuration and the low latitudinal position of Iberia determined central Iberia highs in the southernmost border of Laurasia, beyond which more humid conditions clearly extended towards the equator reaching the present-day Moroccan Meseta and Argana Basin.

*Keywords:* Triassic climates, Buntsandstein, Iberia, Early Triassic, Pangaea

## 1. Introduction

The end-Permian mass extinction devastated both marine and terrestrial ecosystems (Benton, 2003; Erwin, 2006; Algeo et al., 2011). This event, besides being the most catastrophic known loss of biodiversity, was followed by an unusually long period of recovery throughout the Early Triassic (Payne et al., 2004; Kozur and Weems, 2011; Retallack et al., 2011; Benton and Newell, 2014). Takahashi et al. (in press) have even extended to the late Spathian, the global environmental perturbations that were likely responsible for the delayed recovery of life in the marine realm. However, recent studies (Hofmann et al., 2011, 2013) have also suggested that this latter idea should be abandoned.

Although there is increasing evidence indicating that this mass extinction was most probably triggered by a combination of different factors rather than a single event (Bernier, 2002; Galfetti et al., 2007), numerous scenarios related to of the Siberian Traps Eruptions have been proposed (Wignall, 2001; Algeo et al., 2011; Benton and Newell, 2014), including CO<sub>2</sub> emissions and methane release which induced global warming. Recent modelling based on carbon isotope excursions (Payne and Kump, 2007; Kearsey et al., 2009; Romano et al., 2013) supports the latter scenario.

The activity of the Siberian Traps, which continued into Early Triassic times (Nikishin et al., 2002; Payne and Kump, 2007), is interpreted to have led to enhanced greenhouse climate conditions (Retallack et al., 2011; Romano et al., 2013). Global warming is widely thought to have played an important role in biotic crises (Montañez et al., 2007; Benton and Newell, 2014). This factor is considered responsible for intensifying unfavourable conditions for recovering ecosystems during the Early Triassic (Kozur and Weems, 2011), and even described as lethal during this time (Sun

et al., 2012). Although clear connections appear, ecosystem rebuilding and ecological recovery from this period varied between terrestrial and marine realms, and even between regions (Twitchett, 2006). Environmental stress during the Early Triassic in both realms could also have been driven by rapid change between longer intervals of global warming and shorter intervals of global cooling, as observed in faunal change studies (Kozur and Weems, 2011; Posenato, 2008). This interval of time and even the beginning of the Middle Triassic were therefore more complex and nuanced than a simple but dramatic global warming period.

Climate variations between terrestrial and marine realms and different regions were probably related to the particular palaeogeographic configuration of Pangaea (Kiehl and Shields, 2005; Sellwood and Valdes, 2007). Pangaea was approximately centred on the equator, stretching almost from pole to pole and surrounded by the Panthalassa Ocean (Muttoni et al., 2009; Roscher et al., 2011) (Fig. 1). A wide oceanic gulf, the Tethys sea, latitudinally confined to the tropical-subtropical belt, developed on its eastern side. A configuration like this with a vast expanse of exposed land at low and mid-latitudes centred on the equator with a warm Tethys sea would have determined summer heating in circum-Tethyan continental areas with a strong monsoonal regime and extreme continentality. Such a continental climate would have entailed hot summers and relatively cold winters (Kutzbach and Gallimore, 1989), along with a remarkably high tropical sea-surface temperature with peaks of up to 40°C during the Early Triassic (Joachimski et al., 2012).

Despite intense research on the greenhouse climates of Mesozoic times, the climate of the Early Triassic has been relatively ignored until recently. Some decades ago, the Triassic climate was considered that of a general hot-house with ice free poles

without major oscillations. However, recent interesting studies (e.g. Kidder and Worsley, 2004; Sellwood and Valdes, 2007; Galfetti et al., 2007; Twitchett, 2007; Preto et al., 2010; Stefani et al., 2010; Retallack et al., 2011; Bourquin et al., 2011; Sun et al., 2012; Romano et al., 2013; Benton and Newell, 2014, among others) have revealed a more complex scenario with climate oscillations, non-zonal patterns and presence of a global monsoon system.

This contribution considers climate variation over the late Early Triassic - early Middle Triassic time-interval in the Iberian Plate and adjacent areas, its features and palaeogeographical aftermath in the Western Tethys continental realm. Specifically, we examined the effects of these variations on terrestrial life and relationships with pertinent environmental changes and compared our data with those already described for nearby palaeolatitudinal areas.

## **2. Geologic and stratigraphic setting.**

During the Early Triassic, the Iberian plate occupied the eastern flank of the Pangea supercontinent (Fig. 1A) as a small plate close to the southernmost part of the ancient Laurasia megacontinent (Ziegler and Stampfli, 2001; Stampfli and Borel, 2002; Muttoni et al., 2009; Domeier et al., 2012). During the Early Permian, different basins developed on the eastern side of the plate, while the western portion remained stable to form what today constitutes the so-called Hercynian Massif. Basins initially developed as small isolated troughs, but later these gave rise to a complex system of interconnected rift basins in Central and Western Europe during the Early Triassic (van Wees et al., 1998; De Vicente et al., 2009).

The eastern Iberian basins include three main rift systems: the Iberian, Catalan and Pyrenean-Cantabrian basins, or their respective present-day ranges after Cenozoic inversion (Fig. 1B). Some other small basins contemporaneously developed east of the Iberian plate in present-day Sardinia and the Balearic Islands (Ramos, 1995; Bercovici et al., 2009; Cassinis et al., 2003) and show a similar sedimentary record for the Early-early Middle Triassic (Bourquin et al., 2007, 2011; Cassinis et al., 2012; López-Gómez et al., 2012; Galán-Abellán et al., 2013a; Ronchi et al., 2014) (Fig 2). It basically consists of a succession of two-three units of continental origin, each representing one tectono-sedimentary sequence related to different reactivation phases of the rift systems that developed during the Permian (Arche and López-Gómez, 1996; van Wees et al., 1998; Vargas et al., 2009). The succession shows a general fining-upward tendency, and the units may be separated by hiatuses. This continental sedimentary sequence ends with the westward ingression of the Tethys sea across these areas during the middle Anisian (Ziegler, 1988; Kozur and Bachmann, 2008; Bourquin et al., 2011; Escudero-Mozo et al., 2015).

The three units of the tectono-sedimentary cycle are not always recorded in the outcrops of the different basins. However, when they do appear, they show similar sedimentary characteristics and lateral continuity. As across most of Western Europe, the beginning of the Triassic sedimentary cycle is marked by an unconformity on the Upper Permian rocks, representing a time-span of 6–10 m.a. (Bourquin et al., 2011) to 15 m.a. (Durand, 2006).

## *2.1. The Iberian Ranges*

The beginning of the Triassic continental sedimentary cycle in the E Iberian Ranges comprises three lithostratigraphic units (Fig. 2): Valdemeca Conglomerates Unit (VC), Cañizar Sandstones Fm. (CS), and Eslida Mudstones and Sandstones Fm. (EMS). The Valdemeca Unit was initially considered as the lower subunit of the Cañizar Fm. (López-Gómez and Arche, 1993) but later defined as a single unit (De la Horra et al., 2005).

The Cañizar Fm. mostly consists of red-pink, medium-grain arkoses, 80–110 m thick, and laterally corresponds to the Rillo the Gallo Fm. to the west. This formation has been divided into six subunits (C1 to C6) separated by major boundary surfaces (mbs) laterally recognized over hundred kilometres (López-Gómez et al., 2012) (Fig. 3A). It is interpreted as sandy braided fluvial deposits, with some aeolian reworking, evolving to dominantly aeolian deposits in the northern and eastern zones (Soria et al., 2011; López-Gómez et al., 2011). The upper subunits (C5 and C6) are separated from the rest by a prominent major boundary surface (mbs-5) that marks the reactivation of sedimentation and development of a more energetic fluvial system in most of the Iberian Ranges (López-Gómez et al., 2012).

The Eslida Fm. consists of red siltstones and intercalated decimetric sandstone bodies of arkosic composition (Fig. 3B). The formation's thickness is up to 660 m, thinning to the SE and NW, and it is subdivided into six subunits (Ems-1 to Ems-6) based on their sedimentary characteristics (Arche and López-Gómez, 1999). The unit was deposited only in the central-eastern Iberian Ranges, as the western and easternmost areas of the Iberian Basin were elevated during the time of deposition, while the central area experienced intense subsidence (Arche and López-Gómez, 2005). This geographical arrangement has determined marked lateral thickness variations (Fig.

2). As a result of this control, in the sections examined here only the four younger subunits (Ems-3 to Ems-6) of the Eslida Fm. were deposited. The transition of the Eslida Fm. to the first deposits of marine origin is represented by Röt facies, the so-called Marines Fm. (M) in this area, mostly identified through marls, clays and gypsum (Arche and López-Gómez, 1999).

## 2.2. *Pyrenean Ranges*

The beginning of the Triassic continental cycle in the E. Pyrenees (so-called Catalan Pyrenees) was broadly defined as the "Buntsandstein cycle" by Gisbert (1981, 1983), without more detailed subdivisions (Fig. 2). This cycle, which shows an average thickness of about 200 m across the whole area considered, lies, via a marked angular unconformity (30°– 60°), on Permian rocks (Mey et al., 1968; Naetegaal et al., 1969; Gisbert, 1981; Ronchi et al., 2014; Gretter, 2014). The lowermost part of the Buntsandstein consists of coarse-grained conglomerates with deeply erosive base (i.e. the Iguerri member of Naetegaal et al., 1969) and sandstones of gravel braided fluvial systems, channel and aeolian sand-sheets. Overlying these base layers, the upper portion of the Buntsandstein is composed of reddish sandstones, bioturbated mudstones and siltstones of a playa lake environment. Near the top, siltstones and claystones locally change into dark red fine levels until the contact with the Muschelkalk sequence. These "transition" layers probably represent the Röt facies in the Catalan Pyrenees. The contact between the upper fine deposits and dolomites of the first marine incursion probably represents a hiatus that lasts until the Anisian (Escudero-Mozo et al., 2014).



### 2.3. *Catalan Ranges*

The beginning of the Triassic continental sedimentary cycle in the Catalan Ranges is differently represented in the three sectors into which the ranges were subdivided (Calvet and Marzo, 1994). The cycle features three units in each of the three sectors, represented in sections 6, 7 and 8 (Fig. 2), that are broadly considered time-equivalent (Galán-Abellán et al., 2013a). These units, which change in name from south to north, were initially described by Marzo (1986) and more recently by Galán-Abellán et al. (2013a). They are (Fig. 2): Prades Upper Conglomerates (PUC), Prades Lower Sandstones (PLS), and Aragall Sandstones and Mudstones (ASM) in the southern sector; Garraf Upper Conglomerates (GUC), Eramprunyà Sandstones (ES) and Aragall Sandstones and Mudstones (ASM) in the central sector; and Riera de San Jaume Sequence (RSJ) and the Figaró Mudstones and Sandstones (FMS) in the northern sector.

The Prades Conglomerates unit, Garraf Conglomerates unit and the lower part of the San Jaume Sequence were interpreted as deposited by gravelly braided fluvial systems related to proximal alluvial fans. The Prades Sandstones unit was interpreted as fluvio-aeolian deposits, the Eramprunyà Sandstones unit as sandy braided fluvial deposits with intercalated aeolian sandstones, and the upper part of the San Jaume Sequence as sandy braided fluvial deposits. The Aragall and Figaró units were interpreted as mixed-load, sinuous, fluvial systems developed in wide muddy floodplains deposits (Marzo, 1980).

### 2.4. *Sedimentary cycle age*

The sedimentary cycle of the Iberian Ranges has been dated according to palynological assemblages obtained in the Cañizar and Eslida Fms., as well as in the overlying Marines Fm. (Boulouard and Viallard, 1982; Doubinger et al., 1990; Díez et al., 2010), and according to one foraminifer association obtained in, the Landete Fm. (Escudero-Mozo et al., 2015). The base of the Valdemeca Unit has been dated as Smithian, the uppermost Cañizar Fm. is Aegean in age, and the uppermost Eslida Fm. Bithynian (López-Gómez et al., 2012) (Fig. 2).

The equivalent sedimentary cycle in the Catalan Ranges shows a scarce fossil record that consists of a *Pleuromeia* plant specimen in the uppermost part of the Eramprunyà Unit (Galán-Abellán et al., 2013a), and some isolated footprints reptiles and fragments of bones in the El Figarò Unit (Gaete et al., 1994; Fortuny et al., 2011). These are neither sufficient nor representative to indicate the precise age of the beginning of this sedimentation cycle. Díez et al. (2013) examined a pollen assemblage above this cycle, in the Upper Evaporitic Unit (UE) or Röt facies, indicating a Bithynian-Pelsonian age. A magnetostratigraphic study of the cycle in the Riera de San Jaume Sequence (RSJ in Fig. 2) (Dinarès-Turell et al., 2005), assigns the lower part of the cycle to the Spathian and the upper part to the Illyrian. Finally, a precise Pelsonian age obtained for Ammonites in the marine carbonate sediments just above this continental cycle (Escudero-Mozo et al., 2014) (Fig. 2), point roughly to an equivalence between this sedimentary cycle and the one described for the Iberian Ranges.

In the E Pyrenees, an early Anisian age based on palynomorph assemblages (Broutin et al., 1988; Calvet et al., 1993; Díez, 2000; Díez et al., 2005) was obtained for the upper dark red fine clastic deposits of the "Buntsandstein cycle". Based on these palynological studies, we attribute the lower coarser part of this sedimentary cycle a late

Early Triassic age. Thus, the age of this cycle, as well as its general lithological succession would be broadly time-equivalent to those described in both the Iberian and Catalan Ranges (Fig. 2).

### **3. Methods**

The multidisciplinary approach used includes a stratigraphic and sedimentologic study, palaeosol characterisation, and a description of the palaeontologic contents and petrology of fine sediments. Figure 4 shows a scheme of the general data described for the units in the different areas. Given strong correlation between the genesis of many sedimentary rocks and climate change, our stratigraphic and sedimentologic descriptions and interpretations of the units, are based, among other data, on those which allow to obtain temperature, wind direction and precipitation information. Despite the difficulty in obtaining precise ages of continental Triassic rocks, detailed stratigraphic information is necessary as climate change can occur over short time scales, and some continental deposits will not record a specific climate event, as accretion may be very slow (Benton and Newell, 2014).

Based on plant fossils and sediments, our goal was to reconstruct climate variations throughout each unit. This approach was able to identify, for example, correlations between the ecology and growth of floras and different alluvial environments. Preserved palaeosols were used as proxies for precipitation trends and climate seasonality. Further, clay minerals in the profiles examined were used as additional evidence of climate control, as different clay minerals form by chemical weathering under different humidity conditions. Finally, vertebrate ichnites and an

isolated insect data were also used for palaeogeographic reconstruction. All these data were compared with those from near Tethys areas to construct plausible palaeogeographic scenarios for the studied time-interval.

## **4. The sedimentary record**

### *4.1. Stratigraphy and sedimentology*

Our sedimentologic analysis was mostly based on data from prior work on these units, which are here synthesized. Ten selected sections were examined in detail: five in the E Iberian Ranges, two in the E Pyrenees and three in the Catalan Ranges (Fig. 5). Sections commonly show large thickness variations among the different basins. Sedimentation-free areas occur at the basin margins, while prominent depocentres developed away from those areas, where the sedimentary record may approach 400 m in thickness. All sections of the three basins show a hiatus that roughly corresponds to the Aegean but also to the early Bithynian in some cases. This time-span without sedimentation grossly separates coarser from finer siliciclastic sediments, probably related to general plate reorganization, as discussed below.

The depositional systems corresponding to these units were reconstructed through detailed sedimentologic facies description and interpretation. Different architectural elements were also based on facies associations, their hierarchies and stacking pattern characteristics.

The study of the units allowed us to differentiate 19 facies and eight associated or secondary facies. Some of these facies are described according to Miall's nomenclature (1992, 1996); all are summarized in figure 6. Thirteen facies were

ascribed to alluvial sediments, while six (ae1 to ae6) were differentiated into aeolian sediments. These latter facies are locally completed with eight secondary or associated facies.

The facies described as alluvial sediments are basically represented by sandstones, conglomerates or both, while those described in aeolian sediments are basically comprised of sandstones.

Facies and associations between them constitute sedimentary bodies or architectural elements (*sensu* Miall, 1992, 1996), each with a particular external geometry and internal vertical stacking pattern. Sedimentary environments were reconstructed from the analysis and interpretation of these architectural elements. Nine architectural elements identified across the studied units are summarized in figure 7. Six of these elements were related to a fluvial sedimentary environment, and the remaining three to an aeolian sedimentary environment.

The fluvial sedimentary environment includes megaripples, channel fill, lateral accretion, gravel bars, unconfined or semiconfined clast bodies and floodplain architectural elements, while the aeolian sedimentary environment includes dune, sandsheet and interdune architectural elements. The vertical succession of these elements in the studied sections (Fig. 5) reflects sedimentary evolution through the different units and the basins they filled.

Sedimentation in the basins probably started not before the early Smithian. In all cases, the general deposition trend is fining upward. This tendency is interrupted at the boundary between two main cycles of deposition (Fig. 4). The lower one, with a coarser lithology, may start with gravel bar successions (GB), normally amalgamated into

macroforms (Fig. 8a, f). These represent gravelly braided fluvial systems with punctate aeolian reworking in the S Iberian Ranges and Catalan Ranges. Although less frequent, the GM architectural element (Fig. 8b) may also appear in this lower part of the cycle, indicating flash floods or unconfined deposits related to arid or semi-arid climate areas (Durand, 2006, 2008; De la Horra et al., 2005, 2008, 2011; Bourquin et al., 2007, 2011). The upper part of this lower coarser cycle of deposition is basically represented by sandy braided fluvial systems (SB, CH) (Fig. 8c) intercalated into aeolian dune field complexes (E1, E2, E3) that tend to be more frequent towards the central Iberian Ranges and south Catalan Ranges (Figs. 8d, e, h and 9A). In the S Iberian Ranges, above major boundary surface 5 (mbs 5), clear reactivation in the general depositional system allowed for the punctate development of gravel bars in the fluvial systems and a general increase in water fluxes (López-Gómez et al., 2012). Dominant palaeocurrent trends in the E Iberian Ranges point 95°–150° in the fluvial systems and 195°–270° in the aeolian systems. In the Catalan Ranges, dominant palaeocurrents in the fluvial systems point 130°–185°, and are bidirectional 75°–120° and 235°–285° in the aeolian systems. In the E Pyrenees, dominating palaeocurrents trend 275°–320°.

The upper part of the sedimentary cycle is not completely represented in the S Iberian Ranges and, as stated above, only records its four youngest subunits (Ems-3, Ems-4, Ems-5 and Ems-6) in the Cedrillas-Corbalán section, and is even less detectable in the other sections, with a minimum in the Río Mayor section, where this formation was not deposited (Fig. 5). These four subunits are composed of fine sediments with intercalated sandstone levels (Figs. 3b, 8f) that become abundant in Ems-5. They mostly represent sandy braided (SB, CH) fluvial systems crossing huge floodplain (FF) areas where soils developed (Fig. 9B) (Arche and López-Gómez, 2005) and isolated coal

seems in the Castellar N'Hug area (Fig. 5). Some small aeolian dune systems (E1) developed intercalated in the fine deposits in the upper (Ems-6) Torre de Las Arcas - Peñarroyas section, while some sandy meandering (LA) fluvial systems developed in the lower part of the same section (Ems-4). The middle portion of this section (Ems-5), however, represents the reactivation of the whole sedimentary system, with a record reduced in fine deposits and an increase in migrating channels and bar development (Fig. 9C) (Borrueal-Abadía et al., 2014). Punctually, some aeolian reworking is observed in the fluvial systems of the Torre de las Arcas–Peñarroyas section, in subunit Ems-5.

#### 4.2. Mineralogy

Our mineralogical composition study focuses on the Iberian and Catalan Ranges, as there are no data available on the mineral composition of the Triassic units in the selected area of the Pyrenees. In the Iberian Ranges, the mineralogical composition of the Cañizar and Eslida Fms. was firstly described by Alonso-Azcárate et al. (1997) in a general study, and completed in a more detailed study by Galán-Abellán et al. (2013b).

Sandstones from both the Cañizar and Eslida Fms. are quartz-arenites and subarkoses, with quartz, K-feldspar, lithic fragments of slates and phyllites, detrital mica, and accessory phases like rutile, zircon, ilmenite, monazite, apatite, tourmaline and, less frequently, xenotime. The matrix includes illite, hematite and less kaolinite in samples from the eastern sector of the basin, where it is extensively replaced by dickite (Martín-Martín et al., 2007). No primary porosity has been detected, and secondary porosity is filled with kaolinite, quartz, illite and iron oxide cements. In addition, samples from both units contain strontium-rich aluminium phosphate sulphate minerals (APS minerals). However, these phases are more abundant in the basal part of the

Cañizar Fm., where they commonly replace lithic fragments. In samples from the Eslida Fm., these APS minerals occur as tiny ( $>3\ \mu\text{m}$ ) disseminated pseudocubic crystals. Textural relationships strongly suggest that APS minerals are early diagenetic in origin, and precipitated shortly after sedimentation, most probably under the influence of acidic meteoric waters (Galán-Abellán et al., 2013b).

As mentioned before, the Cañizar Fm. is almost exclusively formed by sandstones. On the other hand, the Eslida Fm. includes mudstone and siltstone layers intercalated with sandstones. A remarkable feature of the Eslida Fm. is the local occurrence of carbonate (formed by dolomite or calcite) concretions in some palaeosols within these fine layers. Clay minerals in the mudstones are mainly illite, with minor amounts of pyrophyllite or kaolinite (the latter replaced by dickite), which are more abundant in the eastern sections. The illite crystallinity (IC) data indicate that most sections in the Iberian Ranges reached deep diagenetic conditions ( $0.44^\circ$  to  $0.75^\circ\ \Delta 2\theta$ ; Benito et al., 2005), in agreement with the illite and dickitized kaolinite assemblage. However, the presence of pyrophyllite and lower IC data ( $0.41$  to  $0.28^\circ\ \Delta 2\theta$ ) in some sections (those showing the maximum thickness of the Eslida Fm.) are indicative of very low grade metamorphism (Alonso-Azcárate et al., 1997; Benito et al., 2005).

A preliminary approach to the mineralogical composition of the Early-Middle Triassic rocks of the Catalan Ranges was performed by Galán-Abellán (2011) in the Eramprunyà unit (ES) and Aragall unit (ASM) in the central sector, and in the El Figarò unit (FMS) in the northern sector (Fig. 2). Mineral assemblages are rather similar to those found in the Iberian Ranges, and include quartz, hematite, illite and kaolinite, and



minor amounts of feldspar. Dolomite and calcite rarely occur in the ES, but are frequent in samples from both the ASM and FMS units. APS minerals are also found as accessory phases in some samples. Sandstones and siltstones in the Catalan Ranges show a lower degree of diagenesis, as revealed by IC data. Late diagenetic processes promoted the development of secondary porosity, subsequently cemented by carbonate (calcite and dolomite), which obliterated the original mineral assemblage.

Because of the large proportion of detrital phases and of the deep diagenetic to very low metamorphic conditions, these mineral assemblages cannot be directly used to decipher the palaeoclimatic conditions that prevailed during the sedimentation of these units. However, as will be discussed later, variations in clay mineral formation is related to chemical weathering intensification, a process dependent on atmospheric temperatures (Velde and Meunier, 2008).

## **5. Palaeobotany**

Anisian Triassic plant remains have been recovered in both the Iberian and Catalan Ranges. In the Pyrenean Ranges, palynomorph assemblages have been only reported for the Buntsandstein facies (Broutin et al., 1988; Calvet et al., 1993; Díez, 2000; Díez et al., 2005), indicating an Anisian age. Studies of these records have been scarce but some include a detailed compilation of prior references and provide tentative palaeoenvironmental reconstructions. In the eastern Pyrenees only the palynomorph assemblages previously mentioned and some undetermined flora fragments have been found to date.

### *5.1. Iberian Ranges*

Although without specifying a precise stratigraphic or geographic position, Schmidt (1937, in Dobruskina, 1994), describe a Triassic macroflora in the S Iberian Ranges, identifying *Pleuromeia sternbergii* (Münster) Corda.

There are no reports of macrofloral remains in the Cañizar Fm. (Figs. 5 and 9A). The only remains in the units of the Iberian Ranges examined appear in the Eslida Fm. In this unit, different floral associations indicate an upward decrease in floral diversity. In the Eslida Fm., floral associations types can be distinguished depending on the plant remains found. The first, found in subunits Ems-3 and Ems-4 (Fig. 9B), features a macroflora composed of riparian vegetation including semiarborescent lycophytes (*Pleuromeia*), sphenophytes (at least *Equisetites*, perhaps also *Neocalamites*) and more hygrophytic conifers, such as *Pelourdea* (Borrueal-Abadía et al., 2014) (Fig. 10a, b, c). The vegetation of the lowlands is characterized by drier conditions, where various species of arboreous conifers developed, such as *Voltzia*, and shrubby ones such as *Albertia*. The possible hinterland vegetation consists of conifers along with shrubs (*Albertia*) and trees (*Voltzia*) (Fig. 10d). These associations are laterally arranged but also appear vertically alternating, probably indicating the alternation of drier and more humid conditions, possibly in a seasonal climate, but also indicating a position more or less distal to channels (Borrueal-Abadía et al., 2014).

In subunit Ems-5 of the Eslida Fm., where CH and SB architectural elements dominate, large indeterminate fragments of putative conifers have been found, probably as a result of their greater resistance to transport (Borrueal-Abadía et al., 2014) (Fig. 9C). However, this could also be the outcome of a more sparse vegetation that does not protect soils from erosion. Besides, the presence of conifers only could indicate a shift to more arid conditions, taphonomic selection or a combination of both.

In subunit Ems-6 of the Eslida Fm., only a *Pleuromeia* fragment and specimens of bad preserved *Peltaspermum*, maybe part of a fern with seeds, have been identified. This is striking because in subunits Ems-3 and Ems-4 showing similar sedimentation and preservation characteristics, a larger number of specimens have been discovered. This could be due to arid conditions near inland sabkhas inferred from sedimentologic criteria (Borrueal-Abadía et al., 2014).

The only pollen assemblage described in the Eslida Fm. consists of conifers, ferns and seed ferns, and contains *Podocarpeapollenite*, *Minotosaccus*, *Platysaccus*, *Succintisporites* and *Cristatitriletes* (Boulouard and Viallard, 1982).

In the N Iberian Ranges, in equivalent stratigraphic positions, Díez et al. (1996) and Díez (2000) described a similar Anisian association composed of *Darneya* sp., *Darneya peltata*, *Equisetites* sp., *Neocalamites* sp., *Neocalamites* cf. *carrerei*, *Willsiostrobus* sp., *Willsiostrobus rhomboidalis*, *Pelourdea vogesiaca*, *Albertia* sp., *Voltzia* sp., *Voltzia heterophylla* and *Voltzia walchiaeformis*. In this latter area, two palynomorph assemblages have been described in the Cálcena Fm. (Arribas, 1984) in a possible stratigraphic location equivalent to the upper part of the Eslida Fm., that mainly contains conifers and ferns (*Alisporites*, *Chordasporites*, *Triadispora*, *Verrucosisporites* and *Volziaceasporites*) (Díez et al., 2007).

Palaeoenvironmental reconstructions of these associations point to a riparian vegetation comprising plants living near the water body (permanent floodplain ponds or river) subjected to periodical floods. The vegetation around the water bodies is composed of sphenophytes (*Equisetites* and *Neocalamites*) and hygrophytic conifers such as *Pelourdea* (see also Kustatscher et al., 2014). Further from the water body, lowland vegetation is characterized by drier conditions, and includes various species of

conifers such as *Voltzia*, *Albertia*. Possible hinterland vegetation (permanent ground or seasonally dry) comprises conifers (*Voltzia*, *Albertia*, *Willsiostrobus* and *Darneya*).

## 5.2. Catalan Coastal Ranges

In the Catalan Ranges, the first macrofloral remains appear in the so-called “Lower Buntsandstein”, and take the form of a putative *Pleuromeia*, located in the upper part of the Eramprunyà Unit, which is equivalent to the top of the Cañizar Fm. (Galán-Abellán et al., 2013a).

In the “Upper Buntsandstein”, in green shales with malachite, Almera (1909) described an association composed of remains of *Albertia* sp., *Calamites* sp., *Voltzia heterophylla* and *Pecopteris sulziana*. Two similar bands with macrofloral remains were reported by Calzada (1987). The lower one only contains *Equisetites* sp. and the higher one *Aethophyllum* sp. and *Equisetites* cf. *mougeotti*. Original lithostratigraphic descriptions of the levels where the samples were obtained point to the El Figarò Unit, in a stratigraphically equivalent level towards the top of the Eslida Fm. (Galán-Abellán et al., 2013a).

In the Catalan Ranges (El Figarò Unit), hygrophytic taxa that grew in the wetter areas around ponds and along river banks can also be observed such as sphenophytes (*Equisetites* and *Calamites*) and ferns (*Pecopteris sulziana*). The vegetation of the lowlands is characterized by species of arboreous conifers, such as *Voltzia* and *Aethophyllum*, and shrubby species, such as *Albertia*, as well as ferns in the understory (*Aethophyllum* and *Pecopteris*).

Macrofloral remains found in the Son Serralta Fm. of Majorca (Calafat-Colom, 1988; Álvarez-Ramis et al., 1995) are similar to the ones described in the El Figarò Unit

of the Catalan Ranges, and consist of *Aethophyllum stipulare*, *Albertia* sp., *Anomopteris mougeotti*, *Endolepis* sp., *Equisetites* sp., *Equisetites mougeotii*, *Neuropteridium* sp., *Schizoneura-Echinostachys paradoxa*, *Voltzia heterophylla* Brongniart, *Voltzia walchiaeformis*, *Willsiostrobus hexasacciphorus*, *Willsiostrobus* sp. and *Pelourdea* cf. *vogesiaca*. This assemblage is attributed to the middle Anisian in view of the palynological analysis published by Ramos and Doubinger (1989).

In NW Sardinia, inside a whitish horizon in the Cala Viola sandstones, Pecorini (1962) found estherias and plant remains (*Equisetum* cf. *mougeotii*), and attributed such a formation to the Lower Triassic. Two distinct palynomorph associations of (?)Scythian-early Anisian and late Anisian age from the subsurface are reported in comparable deposits (Pittau and Del Rio, 2002).

## 6. Palaeosols

Our palaeosol study mainly focused on some profiles of the Eslida Fm., in the Gátova stratigraphic section of the Iberian Ranges (Fig. 11). Only levels showing root traces, soil structure, and soil horizons were considered paleosols (Retallack, 1988, 2005). These palaeosols have been differentiated and classified into a field scheme of pedotypes using established criteria (Retallack, 1997). The USDA Soil Taxonomy system (Soil Survey Staff, 1999) was used to define horizons using letters (such as A, Bt and Bk) and to designate diagnostic horizons. The classification of Machette (1985) was used for the state of carbonate accumulation, and the degree of development of the palaeosol was estimated using the scale of Retallack (1988).

The first evidence of pedogenesis was observed at the top of subunit Ems-3 and base of subunit Ems-4, in silty red floodplain facies. Vertical root traces and a thick (5-10 mm) platy structure are related to the thin ochric epipedons and incipient subsurface clayey horizons of pedotype Gat-A (Fig. 11A). Root traces are scarce, short (5-10 cm) and preserved by infills of red or green clay. Dispersed powdery carbonate and carbonate nodules (stage I-II, Machette, 1985) occur in the subsurface clayey horizons, only a few centimetres beneath the soil surface (5-10cm), but this calcareous level does not constitute a calcic (Bk) horizon. Nodules are horizontally elongated (2-5 cm) but thin (0.5-1 cm) and show a lenticular shape. The shallow scarce root traces, the only slightly altered bedding, and short distance to the carbonate disc-shaped nodules are indicative of a sparse vegetation that probably developed under dry conditions for most of the year (Retallack, 2005). These palaeosols represent weakly developed silty to sandy Entisols of flat land surfaces, which were not frequently flooded and developed under arid climates.

The upper part of subunit E4 displays palaeosols at carbonate accumulation stage II-III in the floodplain facies (Machette, 1985). These moderately developed silty red palaeosols are characterized by a partially eroded Bt clayey horizon, from which root traces emanate downwards into a Bk calcic horizon of slightly coalescing carbonate nodules measuring 0.5-2 cm (pedotype Gat-B; Fig. 11B). Columnar and subangular blocky structures are observed in the Bt horizon, which is also burrowed by several channels of roots of small size (up to 12 cm in length). Bk horizon thickness is up to 20 cm and entire profiles are generally 30 to 40 cm. The Gat-B pedotype was classified as an Inceptisol (Soil Survey Staff, 1999).

Under arid climates, thicker Bk horizons are usually interpreted as indicative of a longer time of pedogenic development (Gile et al., 1966). However, in non-extreme arid climates, thicker Bk horizons are the result of seasonal variations in soil wetting depth (Retallack, 2005) and greater plant activity (Alonso-Zarza et al., 2003). As the thickness of the Bk horizon does not exceed 30 cm, there is no evident seasonal variation in rainfall (Retallack, 2005). However, the greater presence of root traces suggests better conditions for plant growth, and, thus, this part of subunit Ems-4 was deposited under conditions of slightly higher mean annual rainfall than for the Ems-3 - Ems-4 transition.

The base of the Ems-5 subunit features palaeosols developed on abandoned channel deposits of the fluvial system (pedotype Gat-C; Fig. 11C). These palaeosols are characterized by poor alteration of the bedding as long root traces penetrate channelized sand bars. The most common type is composed of a single vertical root up to 1.5 m long and 4 cm thick, with rootlets radiating downwards another 20-30 cm from the lower part of the main root (Fig. 11D). This pattern is similar to modern adventitious prop roots that support trees in soft sandy sediments. Also observed were dispersed small lateral roots and main roots or taproots up to 45 cm long and 5 cm thick, with little branching, profuse hair roots, and ending in rounded tap roots (Fig. 11E). Due to poor alteration of the parent material, the sandy Gat-C pedotype was classified as a Fluvent in the order Entisol (Soil Survey Staff, 1999), also possibly indicating high erosion rates and an arid climate. In their study of the palaeoflora of the Eslida Fm., Borrueal-Abadía et al. (2014) found no lycophytes, sphenophytes and hygrophytic conifers in this subunit. As only conifer remains were found, these authors proposed a drier climate (Borrueal-Abadía et al., 2014). However, in spite of this dry climate, the growing well-sized trees were possible in some areas (Fig. 9C).

The E6 subunit is characterized by the presence of silty palaeosols with profuse drab-haloed root traces (Fig. 11). A light red horizon with fine subangular blocky structure lies on top of a clayey Bt horizon with a dense pattern of fibrous root systems. Very few dispersed carbonate nodules were observed at a depth of 35 cm from the profile top. These weakly developed palaeosols do not reach the criteria for Alfisols and were classified as Inceptisols. Drab-haloed root traces are usually interpreted as chemical reduction related to anaerobic bacterial activity in stagnant water (Retallack, 1997). However, the Gat-D pedotype lacks a gleyed superficial horizon and the drab-haloed root traces are probably the outcome of anaerobic decay in the rhizosphere and other areas after burial. Observed features of the Gat-D pedotype (Fig. 11E) point to oxidizing dry soils though periodic waterlogging cannot be ruled out.

In the northern area of the Catalan Ranges, the development of caliche was described by Marzo et al. (1974) and Marzo (1980) in the middle part of the El Figaró unit. This may appear in floodplains or close to meandering channels and was interpreted as early mature caliche resulting from short subaerial exposures in semiarid conditions.

## **7. Discussion**

### *7.1. Climate variations*

Through a detailed study of the sedimentary characteristics and fossil contents of selected lithostratigraphical units of the S Iberian Ranges, E Pyrenees and Catalan Ranges, we were able to identify different phases of climate installation and development during the Early-Middle Triassic. Despite the fact that these basins were hundreds of kilometres apart and adopted their own characteristics during their refill,



common sedimentary features appear in the sedimentary record of the time-interval examined.

Some of these features, described above and shown in figure 5, are provided in figure 12 as climate indicators. The more remarkable indicators detected in most of the studied sections are here considered representative of the entire study area. Punctuate sedimentary characteristics of some sections are used as regional or local climate indicators.

The first sedimentary record of the basins examined starts during the late Smithian and continues in the Spathian until its interruption at the beginning of the Anisian (López-Gómez et al., 2012; Galán-Abellán et al., 2013a; Ronchi et al., 2014). Although it seems there were no clear humid nor subhumid climate stages during that time, remarkable arid and semi-arid climate period alternations were observed. Three clear arid periods, usually well represented by aeolian dune field sedimentation, developed at the end Smithian, transition to the Spathian, middle Spathian and transition to the Aegean (Fig. 12). In addition, several authors (De la Horra et al., 2005, 2008, 2011; Durand, 2006, 2008; Bourquin et al., 2007; 2011; Cassinis et al. 2007) suggest a (hyper)-arid period during the first of these time-intervals when plant remains are absent (Durand, 2006, 2008; Bourquin et al., 2007, 2011). The durations of these three arid phases are probably decreasing from the oldest to the youngest, and thus, involved the development of major semi-arid stages. As the studied Early Triassic time-interval represents about 1.5 m.a., each of the three alternating arid to semi-arid intervals would be shorter than 0.4 m.a. Semi-arid intercalated stages were represented by developing braided fluvial systems in all the basins. In some cases, these depositional systems were

laterally interconnected with the development of small aeolian field dunes (López-Gómez et al., 2012).

The presence of major boundary surface 5 (mbs5) in the different sections of the study basins (Fig. 12), its age and characteristics, was considered as an important regional event (López-Gómez et al., 2012; Galán-Abellán et al., 2013a), probably related to the Hardegsen unconformity described in Western Europe (e.g. Aigner and Bachmann, 1992; Bourquin et al., 2007, 2009) and linked to stages of tectonic activity at the end of the Early Triassic. In our basins, this regional change is also reflected by low angle unconformities in sections near the basin border, and coincides with a more humid stage after an arid episode and the start of life recovery after the Permian-Triassic crisis (López-Gómez et al., 2012).

Despite the development of these generalized and laterally continued climate stages, some areas in the E. Iberian Ranges (Gátova section) and E Pyrenees (Castellar N'Hug) hardly show aeolian sediments. On the contrary, in the southern Catalan Basin (S. Gregori section), almost the whole sedimentary record consists of aeolian sediments. These punctate geographical differences, as detailed below, point to a dishomogeneous climate distribution and to climate control.

After a sedimentary interruption and slight erosion event during the Aegean, a new cycle of sedimentation started at the beginning of the Bithynian (Fig. 12). This new cycle, represented by the Eslida Fm., the "upper Buntsandstein" or El Figarò Unit in the Iberian Ranges, E. Pyrenees and Catalan Ranges, respectively, was related to tectonic reactivation and new re-organization and orientation of the rift basins in Iberia (Arche and López-Gómez, 1996, 2005). Mudstones and siltstones represent the main lithological change compared to the previous cycle. However tectonics was not the only

reason for these lithological variations, and rather, a change in climate allowed for the sedimentation of different deposits and the emergence of new alluvial sedimentary styles.

The development of extensive meandering fluvial systems, and the appearance of sphenophytes, conifers and isolated coal levels in subunits Ems-3 and Ems-4 suggests the presence of the two short humid phases in the middle Bithynian (Fig. 12). These characteristics were widely developed during these stages in different areas of the three study basins. The two humid stages, however, only represented interruptions of a more prolonged period of alternating subhumid and semi-arid stages that lasted until the end of the Bithynian and continued into the beginning of the Pelsonian, when sedimentation of the Röt facies (Marines Fm.) reflects the transition to the first Tethys sea incursion (Muschelkalk facies) in Iberia (Escudero-Mozo et al., 2014). The proximity in time of these two humid stages could mean their interpretation as a single humid interval in some sections.

Based on the sedimentary record, as shown by the frequent reactivation surfaces presence, on the appearance of hinterland vegetation of conifers (*Voltzia*, *Albertia*, *Willsiostrobus* and *Darneya*) and on soil development as the presence of thicker Bk horizons in non-extreme arid conditions, subhumid stages would consist here of seasonal precipitation, whereby extreme temperatures and rainfall were probably not persistent plant development, soil growth and permanent or semi-permanent flows in river systems are described.

However, a short semi-arid stage is inferred at the end of the Bithynian. This stage, which is even represented by small aeolian dunes in the Iberian Basin (Torre de las

Arcas–Peñarroyas section), was also marked by the presence of xerophytic vegetation, and presence of unconfined braided fluvial systems.

## *7.2. Palaeoclimatic and palaeogeographic implications*

The simplistic hot-house scenario for the Early-Middle Triassic, evoking strong monsoon circulation and seasonal rain without zonal patterns (Kiehl and Shields, 2005; Preto et al., 2010), has been recently modified by the incorporation of detailed regional data to define a more complete evolution model for this period of time (Romano et al., 2013; Sun et al., 2012).

Although temperatures had risen rapidly during the end-Permian mass extinction, they reached exceptionally high values in the Early Triassic (Brayard et al., 2010). These high temperatures also experienced large abrupt changes such as that observed in the Smithian-Spathian transition of up to 40° at the equator (Sun et al., 2012), which was probably the consequence of a carbon cycle disturbance caused by a sequence of large-scale CO<sub>2</sub> injections from the Siberian Large Igneous Province (Payne et al., 2004; Galfetti et al., 2007; Romano et al., 2013).

The latest Smithian was a time of warm and equable climate, expressed as an almost flat pole to equator sea surface temperature gradient, compared to the steep gradient at the beginning of the Spathian, indicating clear latitudinally differentiated climate conditions (Kidder and Worsley, 2004; Preto et al., 2010) inducing a synchronous major change in both terrestrial and marine ecosystems (Galfetti et al., 2007). This change was observed in the present study area, where aeolian-fluvial sedimentation at the end of the Smithian underwent a sudden change towards pure fluvial sedimentation of a semi-arid nature at the beginning of the Spathian (Fig. 12) (Bourquin et al., 2011; López-Gómez et al., 2012; Galán-Abellán et al., 2013a).

However, the new fluvial sedimentation trend that started at the beginning of the Spathian in these areas was not permanent as new arid conditions once again arose.

These high temperature values together with their changing character, thwarted ecosystem recovery during the Early Triassic (Retallack et al., 2011; Sun et al., 2012). In the Iberian Plate, no fossil record is known until the late Spathian (López-Gómez et al., 2012; Galán-Abellán et al., 2013a; Borruel-Abadía et al., 2014) (Fig. 12), clearly coinciding with the first recognized humid and cooler stage in the Triassic rocks of this area, about 5 m.a. after the PTB. A taphonomic filter is initially discarded as this absence includes plants, tetrapods, insects, soils and bioturbation. Until this time, arid and semi-arid conditions were mainly the dominant environmental conditions represented in all the study basins, with a remarkable late Smithian arid stage followed by a cooler period in the earliest Spathian. This latter stage may coincide with the marine cooling event related to strong recovery of many clades described by Brayard et al. (2009), Romano et al. (2013), Sun et al. (2012, 2015) and Chen and Benton (2012).

A humid climate stage can enhance subaerial weathering with consequences on ocean nutrient fluxes (Payne et al., 2004; Twitchett, 2007; Algeo and Twitchett, 2010; Benton and Newell, 2014). Higher ocean nutrient levels may initially increase productivity, which indicates continent-ocean connections (Algeo et al., 2011). These latter authors propose a chemical weathering stage by the late Spathian accounting for the marine productivity increase. This stage fits in well with the one postulated for the Iberian plate and its possible extension in Western Europe. Its association with the recovery of continental life described here reinforces the idea of continental-marine connections described by Algeo et al. (2011).

Tectonic activity, as described above, can play a role in opening continental corridors, as could have happened in the Iberian Plate. These new routes appearing in the megacontinent would promote rifting connections and alluvial fluxes, incorporating more oxygenated waters to the sea and contributing to life recovery. Diedrich (2008) described millions of reptile tracks during the Early-Middle Triassic as a consequence of fauna migration across corridors and bridges in Central Europe. In the Iberian and Catalan Ranges, the first reptile tracks were localized in the uppermost Cañizar Fm., latest Spathian (Gand et al., 2010) (Fig. 12), just after the cited unconformity, and were lacertoid three digit prints of *Rhynchosauroides*. Above these levels, and already in the Anisian (mainly Bithynian), footprints of specimens of both Lacertoid and Crocodiloid groups are common (Gand et al., 2010; Fortuny, 2011) and coincide with the appearance of the first Mesozoic (triadotypomorphan) insect in Spain, *rubra* sp. nov. (Béthoux et al., 2009).

Plant fossils have been used for climate reconstruction based on their ecology inferred from living relatives. Climate is commonly recorded in the sedimentary record by vegetation, and the effects this vegetation has on sediment erodibility, sediment yield and channel style, among others (Miall, 1996). The early Anisian floral associations of both the Iberian and Catalan Ranges are similar and mainly composed of conifers and sphenophytes. These floral associations resemble that of the “Grès à *Voltzia*” Fm. of north-eastern France (Grauvogel-Stamm, 1978). It is likely that the plants of the “Grès à *Voltzia*” that already appear in the *Pleuromeia* flora (Fuchs et al., 1991; Mader, 1990; Grauvogel-Stamm, 1999) escaped the end-Permian life crisis in extrabasin refugia. *Pleuromeia*-like fossils reveal that *Pleuromeia* may have survived into the Anisian in the Iberian Ranges. Moreover, as shown by Grauvogel-Stamm and Ash (2005),

lycophytes played an important role in the recovery of land plants in the Early Triassic and could have adapted to unfavourable arid conditions. The replacement of the *Pleuromeia* flora by conifer-dominated or *Voltzia* flora may be the consequence of a change in climate and growth conditions, enabling the *Voltzia* flora to invade basin lowlands (Grauvogel-Stamm and Ash, 2005).

The plant associations of the Iberian and Catalan Ranges point to alternating seasonally dry and more humid conditions (Borrueal-Abadía et al., 2014). Riparian vegetation, that is, plants living near the water body (permanent floodplain ponds or river), was exposed to periodical flooding. The vegetation around the water bodies was composed of semiarborescent lycophytes, sphenophytes and more hygrophytic conifers. Further from the water bodies, lowland vegetation was characterized by drier conditions, where several species of arboreous and shrubby conifers, and ferns grew. Clearings were colonized by ferns mixed with some conifers, and the possible hinterland vegetation (permanent ground or seasonally dry) consisted of conifers with shrubs and trees. The first more humid short stage, recognized in the early Anisian (Bithynian) in both the Iberian and Catalan Ranges sections, appears in subunits Ems-3 and Ems-4 related to a riparian-dominated vegetation.

Such alternations of dry and more humid conditions shown by the vertical distribution of early Anisian plants in the sections examined, fits in well with changes in river channel style in the same units described by Arche and López-Gómez (2005). Further, Borrueal-Abadía et al. (2014) linked fossil plants to different fluvial architectural elements depending on the hygrophytic to semi-arid xerophytic deposition of the Eslida Fm. A second more humid early Anisian (Bithynian) short stage was observed in the Ems-4 subunit of this formation in the Iberian Ranges related to

superimposed meandering fluvial systems and associated riparian vegetation. In similar studies, Smith (1995) interpreted the facies transition in the Permian-Triassic Karoo Basin as a change in fluvial style from meandering to low sinuosity channels with general drying of floodplain habitats. Davis and Gibling (2010) described a sharp increase in the abundance of meandering rivers in the middle Palaeozoic due to colonization of terrestrial environments by vegetation. The soils of the sections here examined formed in the floodplains during long sedimentation pauses.

Although they are poorly developed, pedotype characteristics also revealed clearly alternating climate conditions. According to the information obtained from the Eslida palaeosols, a general trend of seasonal, alternating drier and slightly humid or semi-arid climate conditions was inferred. The unit is represented by poorly developed soils with shallow calcareous horizons in the lower part of the Eslida Fm. indicative of arid conditions (pedotypes Gat-A), which moved towards slightly higher mean annual palaeoprecipitation (pedotype Gat-B) and possibly better conditions for tree growth (Gat-C). The top of the unit is marked by pedotype Gat-D, with a dense and laterally continuous pattern of fibrous root systems, indicating a well-developed vegetative cover formed under a more seasonally semi-arid climate. Despite such different climate conditions, however, it is difficult to identify clear monsoon characteristics in the sedimentary record, as they can be easily confused with other seasonal effects (Miall, 1996).

Faster soil reaction rates in the Anisian cycle of sedimentation in response to warmer temperatures probably intensified chemical weathering (e.g. Korte et al., 2005) providing clay minerals as crucial data for inferring palaeoclimates. This type of mineralogy has been frequently used to detect changes in the climate conditions



prevailing during their sedimentation (Righi and Meunier, 1995; Hong et al., 2007; Wang et al., 2013). However, diagenetic alteration and source rock composition should always be considered (Chamley, 1989; Hillier, 1995; Yakimenco et al., 2000). The mineral assemblages of the Cañizar and Eslida Fms. in the Iberian Ranges can hardly be used for this purpose, as the original clay mineralogy has been largely obliterated by deep diagenetic and even very low grade metamorphic processes, as evidenced by the presence of dickite and pyrophyllite, respectively, and by illite crystallinity data. In the Catalan Ranges, the generation of secondary porosity and subsequent carbonate cement precipitation during late diagenesis also make it difficult to recognize the original mineral assemblage. In addition, most clay minerals in these units are probably detrital (Alonso-Azcárate et al., 1997) even in the clay fraction, and it is hard to distinguish between authigenic and detrital particles. Consequently, the mineral cannot be linked to a specific climate. However, the presence of pyrophyllite or dickite in samples from both units can be regarded as indirect evidence of the presence of kaolinite in the original clay mineral assemblage, which would have been transformed during diagenesis or very low grade metamorphism. According to Martín-Martín et al. (2007) and Galán-Abellán et al. (2013b), kaolinite formed by weathering of detrital micas and to a lesser extent of K-feldspar, and this alteration implies relatively humid conditions and low pH values to allow for the hydrolysis of these phases. These low pH values, probably the outcome of higher levels of atmospheric CO<sub>2</sub> along with volcanic SO<sub>2</sub> release (Wignall, 2007; Self et al., 2008), are indicated by the presence of APS minerals in both the Cañizar and the Eslida Fms. (Galán-Abellán et al., 2013b). Indeed, a low pH could have been an additional environmental stressor for continental biota.

During the end of the Early Triassic, the Iberian plate was located in the northern hemisphere, facing the Tethys between 10°N and 14°N (Dinarés-Turell et al., 2005; Bourquin et al., 2011; Domeier et al., 2012). Interestingly, the latitudinal position of Iberia during the Early Triassic was one of generally wetter conditions than most of the rest of Europe (Fig. 13). During this time, river systems flowed to the sea, but punctually these systems were interrupted by aeolian dune fields (Galán-Abellán et al., 2013a). These interruptions, nevertheless, diminished in time and space during the beginning of the Anisian, when alternating wet-dry conditions prevailed.

The Iberian plate had different climate domains of irregular extension arising from its pronounced orography. The Iberian plate, being part of the ancient boundary between Gondwana and Laurasia during the assembly of Pangea, experienced significant deformation identified in part of the highly curved Variscan belt of southwestern Europe (Weil et al., 2001; Martínez-Catalán, 2011). Such intense deformation led to the development of mountain belts continuing well into the Permian and even Early-Middle Triassic (López-Gómez et al., 2012). Mountain orography induces atmospheric circulation changes. Fluteau et al. (2001) compared different palaeogeographic scenarios in the Late Permian by testing palaeo-elevations through sensitivity experiments. These authors noted a substantial increase in aridity in the elevated Variscan belt that contributed to the development of aeolian facies and xeromorphic vegetation. These latter authors also estimated an altitude between 2000 - 3000 m in southern Europe for the Late Permian, elevations that persisted until the Olenekian controlling climate and palaeodrainages (Bourquin et al., 2011). The tectonic influence on climate has been evidenced either during Triassic times by Oyarzum et al. (1999) and Fluteau (2003).

Three important highs controlled climate change in Iberia during the Late Triassic: the Ateca-Montalbán High (AMH), Ebro High (EH) and Girona High (GH) (Fig. 13). These elevated areas and dominant E and NE winds led to the development of the alluvial systems and aeolian dune fields represented by the Cañizar Fm. in the Iberian Ranges (López-Gómez et al., 2012), Eramprunyà Unit in the Catalan Ranges (Galán-Abellán et al., 2013a) or the "Upper Buntsandstein" in the E Pyrenees Ranges. These palaeohighs, differing in their palaeogeographic morphology, size and orientation, allowed for the development of a vast dune field area enclosed between the Ebro and the Ateca-Montalbán Highs in the middle Spathian (Fig. 13). Fluvial systems were simultaneously surrounding these dune fields across narrow corridors, and most probably they never reached the Tethys developing an endorreheic system. South of the Ateca-Montalbán High, however, practically no aeolian sands were deposited except in punctuate levels of isolated areas (Galán-Abellán et al., 2013a).

This arid period of the middle Spathian alternated with semiarid periods (Fig. 12). During the latter intervals, fluvial drainage was more extensive and most of dune field areas disappeared or were reduced to smaller areas (Fig. 12). In the late Spathian and early Anisian, more humid periods appeared and plants and animals started to colonize.

The Ateca-Montalbán High was a geographical boundary with the more humid areas towards the equator, in the E Argana Basin (Morocco). Here, no aeolian sediments were recorded during the Early Triassic (Tourani et al., 2010; Klein et al., 2010). These climate boundaries are consistent with mean annual precipitation simulations by Bourquin et al. (2007), indicating more than double precipitation in Argana with respect to the Iberian Plate (from <0.1 mm/day to >1 mm/day) during the Olenekian. In

contrast, more extensive arid areas than those of the Iberian plate developed during this time in Central and Southern Europe (Bourquin et al., 2009, 2011). Interestingly, the first tetrapod footprints in the Iberian Plate are recorded in the early Anisian (Fortuny, 2011) during a more humid period, probably as result of migrations from the still prevailing more arid conditions of central Europe.

As previously exposed, the causes driving the inferred climate changes during the Early Triassic have been broadly discussed by different authors, including those related to different volcanism pulses in Siberia. In the Iberian Plate, and probably in neighboring Western Europe areas, tectonics related to the Hardegsen event could have also reactivated already elevated areas. This new palaeogeographic scenario could allow the opening of corridors in land favoring the development and reactivation of drainage networks and the beginning a more humid episode at the end of the Spathian, also favored by the near equator latitudinal position of Iberia. These circumstances, humidity, corridors and more oxygenated waters would have contributed to the fauna and flora recovery in these basins at the end of the Early Triassic.

## **8. Conclusions**

The continental rocks (Buntsandstein facies) and fossils of eastern Iberia's basins provide insight into the climate of the western Tethys domain during the Early-Middle Triassic. This study suggests climate variations for these near equator (10°–14°N) areas.

The Early Triassic was mainly dominated by alternating periods, normally shorter than 0.4 m.a., of arid to semi-arid climates. Two main arid periods marked by aeolian field dune development occurred at the end of the Smithian and middle of the Spathian.

The late Spathian features a first short subhumid to semi-arid period in Iberia just after an unconformity related to the western European tectonically induced Hardegsen event that could be related with the beginning of fauna and flora recovery in the study basins. After another short arid period at the end of the Olenekian, the beginning of the Anisian (Aegean) was marked by short periods of alternating arid and semi-arid to subhumid intervals. The Bithynian and Pelsonian clearly represent a wetter time, showing alternating semi-arid to subhumid intervals interrupted by two short humid episodes in the late Bithynian but also a short isolated arid interval near the Bithynian/Pelsonian boundary.

Climates in Iberia during this period of time were clearly conditioned by relict Variscan. As a result, isolated internal climate zones separated by elevated areas appeared. South of the Ateca-Montalbán High, the generalized wetter climate during the late Olenekian - early Anisian extended towards the equator to the present-day Moroccan Meseta and Argana Basin.

## **Acknowledgements**

We thank David J. Bottjer (Editor), Spencer G. Lucas (Albuquerque, New Mexico) and an anonymous reviewer for providing helpful recommendations to improve this manuscript. This work was supported by a FPI predoctoral contract held by V.B-A. and by project grant CGL2008-24408 awarded by the Spanish Ministry of Economy and Competitiveness. This paper is also a contribution to the following research projects: "Sistemas Sedimentarios y Variabilidad Climática" (642853) of the CSIC, and Basin Analysis (910429), and Palaeoclimatology and Global Change (910198) of the Universidad Complutense de Madrid. Part of the macroflora information was obtained with the collaboration of Evelyn Kustatcher and Carmen

Díeguez and previously published in Borrueal-Abadía et al. (2014). We thank A. Burton for revising the English version of the manuscript.

## References

Aigner, T., Bachmann, G.H., 1992. Sequence-stratigraphic framework of the German Triassic. *Sedimentary Geology* 80, 115–135.

Algeo, T.J., Twitchett, R.J., 2010. Anomalous Early Triassic sediment fluxes due to elevated weathering rates and their biological consequences. *Geology* 38, 1023-1026.

Algeo, T. J., Chen, Z., Fraiser, M., Twitchett, R. J., 2011. Terrestrial-marine teleconnections in the collapse and rebuilding of Early Triassic marine ecosystems. *Palaeogeography, Palaeoclimatology, Palaeoecology* 308, 1–11.

Allen, J.P., Fielding, C.R. 2007. Sedimentology and stratigraphic architecture of the Late Permian Betts Creek Beds, Queensland, Australia. *Sedimentary Geology* 202, 5–34.

Almera, L., 1909. Descubrimient de una de les antigues floras triássicas. *Bulletí de la Institució Catalana d'Historia Natural* 9, 11–14.

Alonso-Azcárate, J., Arche, A., Barrenechea, J.F., López-Gómez, J., Luque, J., Rodas, M., 1997. Palaeogeographical significance of the clay minerals in the Permian and Triassic sediments of the SE Iberian Ranges. *Palaeogeography, Palaeoclimatology, Palaeoecology* 136, 309–330.

Alonso-Zarza, A.M., 2003. Palaeoenvironmental significance of palustrine carbonates and calcretes in the geological record. *Earth–Sci. Rev.*, 60, 261–298.

892 Álvarez-Ramis, C., Fernández-Marrón, M. T., Calafat, F., 1995. Avance sobre la  
 893 megaflora triásica en facies germánica de Estellencs (sector noroccidental de la Sierra  
 894 de Tramuntana, Lallorca). *Revista Española de Paleontología*, número extraordinario  
 895 Homenaje al Doctor Guillermo Colom, 55–58.

896 Arche, A., López-Gómez, J., 1996. Origin of the Permian-Triassic Iberian Basin,  
 897 Central Spain. *Tectonophysics* 266, 433–464

898 Arche, A., López-Gómez, J., 1999. Subsidence rates and fluvial architecture of rift-  
 899 related Permian and Triassic alluvial sediments of the southeastern Iberian Range,  
 900 Eastern Spain. In: Smith, N.D., Rodgers, N. (Eds.), *Fluvial Sedimentology VI*, Spec.  
 901 Publ. Int. Ass. Sedimentology 28, pp. 283–384.

902 Arche, A., López-Gómez, J., 2005. Sudden changes in fluvial style across the Permian-  
 903 Triassic boundary in the Eastern Iberian Ranges, Spain: analysis of possible causes.  
 904 *Palaeogeography, Palaeoclimatology, Palaeoecology* 229, 104–126.

905 Arribas, J., 1984. *Sedimentología y diagénesis del Buntsandstein y Muschelkalk de la*  
 906 *Rama Aragonesa de la Cordillera Ibérica (provincias de Soria y Zaragoza)*. PhD thesis,  
 907 Universidad Complutense, Madrid. Unpublished

908 Baucon A., Ronchi A., Felletti F., Neto de Carvalho, C., 2014. Evolution of  
 909 Crustaceans at the edge of the end-Permian crisis: ichnonetwork analysis of the fluvial  
 910 succession of Nurra (Permian-Triassic, Sardinia, Italy). *Palaeogeography*  
 911 *Palaeoclimatology Palaeoecology* 410, 74–103.

912

913 Benton, M. J., 2003. *When life nearly died. The greatest mass extinction of all Time.*  
 914 *Thames & Hudson, London, 336 p.*

Benton, M., Newell, A., 2014. Impacts of global warming on Permo-Triassic terrestrial ecosystems. *Gondwana Research* 25 (4), 1308–1337.

Bercovici, A., Díez, J. B., Broutin, J., Bourquin, S., Linol, B., Villanueva-Amadoz, U., López-Gómez, J., Durand, M., 2009. Paleobotanical aspects of the Upper Permian (Thuringian) of Minorca (Balearic Islands, Spain): biostratigraphical, biogeographical and paleoclimatic implications. *Rev. Paleobot. Palynol* 158, 14–28.

Berner, R. A., 2002. Examination of hypotheses for the Permo-Triassic boundary extinction by carbon cycle modeling. *Proc. Natl. Acad. Sci. USA*. 99, 4172–4177.

Best, J.L., Ashworth, P.J., Bristow, C.S., Roden, J., 2003. Three-dimensional sedimentary architecture of a large, mid-channel sand braid bar, Jamuna River, Bangladesh. *Journal of Sedimentary Research* 73 (4), 516–530.

Béthoux, O., De La Horra, R., Benito, M. B., Barrenechea, J. M., Galán-Abellán, B., López-Gómez, J., 2009. A new triadotypomorph insect from the Anisian (Middle Triassic), Buntsandstein facies, Spain. *Journal of Iberian Geology* 35 (2), 179–184.

Blodgett, R. H., Stanley, K.O., 1980. Stratification bedforms and discharge relations of the Platte braided system, Nebraska. *Journal of Sedimentary Petrology* 50, 139–148.



937 Borruel-Abadía, V., Galán-Abellán, A.B., Kustatscher, E., Diéguez, C., López-Gómez,  
 938 J., De la Horra, R., Barrenechea, J.F., Arche, A., 2014. Palaeoenvironmental  
 939 reconstruction of the early Anisian from sedimentology and plant remains in the SE  
 940 Iberian Range (E. Spain). *Palaeogeography, Palaeoclimatology, Palaeoecology* 414,  
 941 352–369.

942 Boulouard, C., Viallard, P., 1982. Reduction or lacune du Trias inférieur la bordure  
 943 méditerranéenne de la Chaîne Ibérique: arguments palynologiques. *Comptes Rendus de*  
 944 *l'Académie des Sciences de Paris* 295, 115–123.

945

946 Bourquin, S., Bercovici, A., López-Gómez, J., Díez, J.B., Broutin, J., Ronchi, A.,  
 947 Durand, M., Arche, A., Linol, B., Amour, F., 2011. The Permian-Triassic transition and  
 948 the onset of Mesozoic sedimentation at the northwestern peri-Tethyan domain scale:  
 949 Palaeogeographic maps and geodynamic implications. *Palaeogeography,*  
 950 *Palaeoclimatology, Palaeoecology* 299, 265–280.

951 Bourquin, S., Durand, M., Díez, J. B., Broutin, J., Fluteau, F., 2007. The Permian-  
 952 Triassic boundary and Lower Triassic sedimentation in the Western European Basins:  
 953 an overview. *Journal of Iberian Geology* 33, 221–236.

954 Bourquin, S., Guillocheau, F., Péron, S., 2009. Braided river within an arid alluvial  
 955 plain (example from the Early Triassic, western German Basin): criteria of recognition  
 956 and expression of stratigraphic cycles. *Sedimentology* 56, 2235–2264.

957

958 Brayard, A., Escarguel, G., Bucher, H., Monnet, C., Brühwiller, T., Goudemand, N.,  
 959 Galfetti, T., Guex, J., 2009. Good genes and good luck: ammonoid diversity and the end  
 960 Permian mass extinction. *Science* 325, 1118–1121.  
 961  
 962 Bristow, C.S., 1993. Sedimentary structures exposed in bar tops in the Brahmaputra  
 963 River, Bangladesh. In: Best, J.L., Bristow, C.S. (Eds.), *Braided Rivers*. Geol. Soc. Lond.  
 964 Spec Publ. 75, 277–289.  
 965  
 966 Brookfield, M.E., 1992. Eolian systems. In: Walker, R.G., James, N.P. (Eds.), *Facies*  
 967 *Models. Response to sea level change*. Geological Association of Canada pp. 143–156.  
 968  
 969 Broutin, J., Doubinger, J., Gisbert, J., Satta-Pasini, S., 1988. Premières datations  
 970 palynologiques dans les faciès Buntsandstein des Pyrénées catalanes espagnoles.  
 971 *Comptes Rendus de l'Académie des Sciences de Paris* 2, 159–163.  
 972  
 973 Calafat-Colom, F.J., 1988. Estratigrafía y sedimentología de la litofacies Buntsandstein  
 974 de Mallorca. PhD. Thesis. Barcelona University. 125 p. Unpublished  
 975  
 976 Calvet, F., Marzo, M., 1994. El Triásico de las Cordilleras Catalanas: Estratigrafía,  
 977 sedimentología y análisis secuencial. In: A. Arche (Ed.), *Conferencia de Estratigrafía y*  
 978 *Paleogeografía de España*. Cuenca. Field Trip Guide. 55p.  
 979  
 980 Calvet, F., Solé de Porta, N., Salvany, J.M., 1993. Cronoestratigrafía (Palinología) del  
 Triásico sudpirenaico y del Pirineo Vasco-Cantábrico. *Acta Geologica Hispanica* 28,  
 33–48.

981 Calzada, S., 1987. Niveles fosilíferos de la facies Buntsandstein (Trias) en el sector  
 982 norte de los Catalánides. Cuadernos de Geología Ibérica 11, 256–271.

983

984 Cassinis G., Durand M., Ronchi A., 2003. Permian-Triassic continental sequences of  
 985 northwest Sardinia and south Provence: stratigraphic correlations and palaeogeographic  
 986 implications. In: Decandia, F.A., Cassinis, G. Spina, A. (Eds.), Late Palaeozoic to Early  
 987 Mesozoic events of Mediterranean Europe, and additional regional reports. Spec. Proc.  
 988 Int. Meeting, Siena, 2001. Boll. Soc. Geol. It., Spec. 2, 119–129.

989

990 Cassinis G., Durand M., Ronchi A., 2007. Remarks on the Permian and Permian-  
 991 Triassic boundary in central and eastern Lombardy (Southern Alps, Italy). Journal of  
 992 Iberian Geology 33 (2), 133–142.

993

994 Cassinis, G., Perotti, C., Ronchi. A., 2012. Permian continental basins in the Southern  
 995 Alps (Italy) and Peri-Mediterranean correlations. International Journal of Earth Sciences  
 996 101, 129–150.

997

998 Chen, Z. Q., Benton, M., 2012. The timing and pattern of biotic recovery following the  
 999 end-Permian mass extinction. Nature geoscience 5, 375–383.

1000

1001 Davies, N.S., Gibling, M.R., 2010. Paleozoic vegetation and the Silurian-Devonian rise  
 1002 of fluvial lateral accretion sets. Geology 38, 51–54.

1003 De la Horra, R., Benito, M.I., López-Gómez, J., Arche, A., Barrenechea, J.F., Luque, J.,  
 1004 2008. Palaeoenvironmental significance of Late Permian Paleosols in SE Iberian  
 1005 Ranges, Spain. *Sedimentology* 55, 1849–1873.  
 1006  
 1007 De la Horra, R., Galán-Abellán, B., López-Gómez, J., Sheldon, N.D., Barrenechea, J.F.,  
 1008 Luque, J., Arche, A., Benito, M.I., 2012. Palaeoecological, palaeoenvironmental  
 1009 changes during the continental Middle-Late Permian transition at the SE Iberian  
 1010 Ranges, Spain. *Global and Planetary Change* 94–95, 46–61.  
 1011  
 1012 De la Horra, R., López-Gómez, J., Arche, A., 2005. Caracterización de la Unidad  
 1013 Conglomerados de Valdemeca en la transición Pérmico-Triásico de la Cordillera Ibérica  
 1014 centro-oriental. *Geotemas* 8, 141–145.  
 1015  
 1016 De Vicente, G., Vegas, R., Muñoz-Martín, A., Van Wees, J.D., Casa-Sainz, A., Sopena,  
 1017 A., Sánchez-Moya, Y., Arche, A., López-Gómez, J., Olaiz, A., Fernández-Lozano, J.,  
 1018 2009. Oblique strain partitioning and transpression on an inverted rift: The Castillian  
 1019 Branch of the Iberian Chain. *Tectonophysics* 470, 224–242.  
 1020 Dercourt, J., Ricou, L. E., Vrielynck, B., 1993. Atlas Tethys palaeoenvironmental maps.  
 1021 Beicip- Fronlab, Rueil Malnaison.  
 1022  
 1023 Diedrich, C., 2008. Millions of reptile tracks-Early to Middle Triassic carbonate tidal  
 1024 flat migration bridges of Central Europe-reptile immigration into the Germanic Basin.  
 1025 *Palaeogeography, Palaeoclimatology, Palaeoecology* 259, 410–423.  
 1026

- 1027 Díez J B., Broutin J., Grauvogel-Stamm, L., Bourquin S., Bercovici, Ferrer J., 2010.  
 1028 Anisian Floras from the NE of Iberian Penninsula and Baléaric Island: a synthesis.  
 1029 Review of Paleobotany and Palynology 162, 522–542.
- 1030 Díez, J. B., Bourquin, S., Broutin, J., Ferrer, J., 2007. The Iberian Permian Triassic  
 1031 "Buntsandstein" of the Artagonian branch of the Iberian range (Spain) in the West-  
 1032 European sequence stratigraphical framework: a combined palynological and  
 1033 sedimentological approach. Bol. Soc. géol. Fr. 178 (3), 187–203.
- 1034
- 1035 Díez, J.B., 2000. Geología y Paleobotánica de la Facies Buntsandstein en la Rama  
 1036 Aragonesa de la Cordillera Ibérica. Implicaciones bioestratigráficas en el Perithetys  
 1037 Occidental. Ph.D Thesis. Universidad de Zaragoza (Spain) and Univ. Paris 6, (France).  
 1038 Unpublished.
- 1039 Díez, J.B., Arche, A., Broutin, J., Bourquin, J., De la Horra, R., Ferrer, J., García-Gil,  
 1040 S., López-Gómez, J. (2013). Palynostratigraphical data of the Buntsandstein and  
 1041 Muschelkalk facies from the Iberian Ranges (Spain). Ciencias da Terra VII, p. 170.
- 1042
- 1043 Díez, J.B., Grauvogel-Stamm, L., Broutin, J., Ferrer, J., Gisbert, J., Liñán, E., 1996.  
 1044 Première découverte d'une paléoflore anisienne dans le faciès "Buntsandstein" de la  
 1045 branche aragonaise de la Cordillère Iberique (Espagne). C. R. Acad. Sci. Paris 323 (2),  
 1046 341–347.
- 1047
- 1048 Dinarès-Terell, J., Díez, J.B., Rey, D., Arnal, I., 2005. "Buntsandstein"  
 1049 magnetostratigraphy and biostratigraphic reappraisal from eastern Iberia: Early-Middle

1050 Triassic stage boundary definitions through correlation to tethyan sections.  
 1051 Palaeogeography, Palaeoclimatology, Palaeoecology 229, 158–177.  
 1052  
 1053 Dobruskina, I. A., 1994. Triassic floras of Eurasia. Österreichische Akademie der.  
 1054 Wissenschaften. Schriftenreihe der Erdwissenschaftlichen Kommissionen 10, 1–422.  
 1055  
 1056 Domeier M., Van der Voo R., H. Torsvik T., 2012. Paleomagnetism and Pangea: The  
 1057 road to reconciliation. Tectonophysics 514–517, 14–43.  
 1058  
 1059 Doubinger, J., López-Gómez, J., Arche, A., 1990. Pollen and spores from the Permian  
 1060 and Triassic sediments of the southeastern Iberian Ranges, Cueva de Hierro (Cuenca) to  
 1061 Chelva-Manzanera (Valencia-Teruel) region, Spain. Review of Palaeobotany and  
 1062 Palynology 66, 25–45.  
 1063 Durand, M., 2006. The problem of transition from the Permian to the Triassic series in  
 1064 southeastern France: comparison with other Peritethyan regions. In: Lucas, S.G.,  
 1065 Cassinis, G., Schneider, J.W. (Eds.), Non-Marine Permian Biostratigraphy and  
 1066 Biochronology. Geol. Soc. Spec. Publ. 265, London, pp. 281–296.  
 1067  
 1068 Durand, M., 2008. Permian to Triassic continental successions in southern Provence  
 1069 (France): an overview. Boll. Soc. Geol. Ital. (Ital. J. Geosci.) 127, 697–716.  
 1070  
 1071 Erwin, D.H., 2006. Extinction. How Life on Earth Nearly Ended 250 Million Years  
 1072 Ago. Princeton University Press. Princeton, Oxford. 296 p.

1073 Escudero-Escudero, M.J., Márquez-Aliaga, A., Goy, A., Martín-Chivelet, J., López-  
 1074 Gómez, J., Márquez, L., Arche, A., Plasencia, P., Pla, C., Marzo, M., Sánchez-  
 1075 Fernández, D., 2015. Middle Triassic carbonate platforms in eastern Iberia: Evolution of  
 1076 their fauna and palaeogeographic significance in the western Tethys. *Palaeogeography,*  
 1077 *Palaeoclimatology, Palaeoecology* 417, 236–260.  
 1078  
 1079 Escudero-Mozo, M.J., Martín-Chivelet, J., Goy, A., López-Gómez, J., 2014. Middle-  
 1080 Upper Triassic carbonate platforms in Minorca (Balearic Islands): implications for  
 1081 western Tethys correlations. *Sedimentary Geology* 310, 41–58.  
 1082  
 1083 Fielding, C., Allen, J.P., Alexander, J., Gibling, M.R., 2009. Facies model for fluvial  
 1084 systems in the seasonal tropics and subtropics. *Geology* 37 (7), 623–626.  
 1085  
 1086 Flueau, F., 2003. Earth dynamics and climate changes. *Comptes Rendus Geoscience*  
 1087 335, 157-174.  
 1088  
 1089 Fluteau, F., Besse, J., Broutin, J., Ramstein, G., 2001. The Late Permian climate. What  
 1090 can be inferred from climate modelling concerning Pangea scenarios and Hercynian  
 1091 range altitude? *Palaeogeography, Palaeoclimatology, Palaeoecology* 167, 39–71.  
 1092  
 1093 Fortuny, J., Bolet, A., Sellés, A. G., Cartanyá, J., Galobart, À., 2011. New insights on  
 1094 the Permian and Triassic vertebrates from the Iberian Peninsula with emphasis on the  
 1095 Pyrenean and Catalanian basins. *Journal of Iberian Geology* 37 (1), 65–86.  
 1096

1097 Fuchs, G., Grauvogel-Stamm, L., Mader, D., 1991. Une remarquable flore à *Pluromeia*  
 1098 et *Anomopteris mougeotti* in situ du Buntsandstein moyen (Trias inférieur) de l'Eifel  
 1099 (R.F. Allemagne). Morphologie, paléoécologie et paléogéographie, Palaeontographica  
 1100 222, 89–120.  
 1101  
 1102 Gaete, R., Galobart, A., Palomar, J., Marzo, M., 1994. Hallazgo de Paratosuchus sp.  
 1103 (Amphibia, Temnospondyli) en facies Buntsandstein del Pla de la Calma (Cordilleras  
 1104 Costero Catalanas): Resultados preliminares. Geogaceta 16, 61–63.  
 1105  
 1106 Galán-Abellán, B., 2011. Variaciones sedimentarias, mineralógicas, geoquímicas y  
 1107 bióticas en el Triásico Inferior-Medio (en facies Buntsandstein) de las cordilleras  
 1108 Ibérica SE y Costero Catalana: Implicaciones en la recuperación de la crisis Permo-  
 1109 Triásica. PhD Thesis. Universidad Complutense de Madrid. 295 p. Unpublished.  
 1110  
 1111 Galán-Abellán, B., López-Gómez, J., Barrenechea, J.F., Marzo, M., De la Horra, R.,  
 1112 Arche, A., 2013a. The beginning of the Buntsandstein cycle (Early-Middle Triassic) in  
 1113 the Catalan Ranges, NE Spain: Sedimentary and palaeogeographic implications.  
 1114 Sedimentary Geology 296, 86–102.  
 1115  
 1116 Galán-Abellán, B., Alonso-Azcárate, J., Newton, R.J., Bottrell, S., Barrenechea, J.F.,  
 1117 Benito, I., De la Horra, R., López-Gómez, J., Luque, J., 2013b. Sources of Sr and S in  
 1118 aluminium-phosphate- sulphate minerals in Early-Middle Triassic sandstones (Iberian  
 1119 Ranges, Spain) and palaeontological implications for the west Tethys. Jour. Sed. Res.  
 83, 406–426.



1120 Galfetti, T., Hochuli, P., Brayard, A., Bucher, H., Weissert, H., Os Vigran, J., 2007.  
 1121 Smithian-Spathian boundary event: Evidence for global climatic change in the wake of  
 1122 the end-Permian biotic crisis. *Geology* 35 (4), 291–294

1123 Gand, G., De la Horra, R., Galán-Abellán, B., López-Gómez, J., Barrenechea, J., Arche,  
 1124 A., Benito, M.I., 2010. New ichnites from the Middle Triassic of the Iberian Ranges  
 1125 (Spain): Paleoenvironmental and palaeogeographical implications. *Hist. Biol.* 22 (1-3),  
 1126 40–56.

1127 Gile, L.H., Peterson, F.F., Grossman, J.B., 1966. Morphological and genetic sequences  
 1128 of carbonate accumulation in desert soils. *Soil Science* 101, 347–360.

1129 Gisbert, J., 1981. Estudio geológico-petrológico del Estefaniense-Pérmico de la Sierra  
 1130 del Cadí (Pirineo de érida). PhD Thesis. Univ. Zaragoza. Unpublished.  
 1131

1132 Gisbert, J., 1983. El Pérmico de los Pirineos españoles. In: Martínez García, E. (Ed.),  
 1133 Carbonífero y Pérmico de España. Ministerio de Industria y Energía, España, pp. 405–  
 1134 420.  
 1135

1136 Golonka, J., Ford, D., 2000. Pangean (Late Carboniferous-Middle Jurassic)  
 1137 paleoenvironment and lithofacies. *Palaeogeography, Palaeoclimatology, Palaeoecology*  
 1138 161, 1–34.  
 1139

1140 Grauvogel-Stamm, L., Ash, S.R., 2005. Recovery of the Triassic land flora from the  
 1141 end-Permian life crisis. *C.R. Palevol* 4, 593–608.  
 1142

1143 Gretter, N., 2014. The Permian-Triassic stratigraphic evolution in selected Peri-  
 1144 Tethyan areas: facies analysis and U-Pb geochronology. PhD Thesis, Università di  
 1145 Pavia. Unpublished.  
 1146  
 1147 Hajek, E. A., Edmonds, D. A., 2014. Is river avulsion style controlled by floodplain  
 1148 morphodynamics? *Geology* 42 (3), 199–202.  
 1149  
 1150 Hajek, E. A., Heller, P. L., Sheets, B. A., 2010. Significance of channel-belt clustering  
 1151 in alluvial basins. *Geology* 38 (6), 535–538.  
 1152  
 1153 Hasiotis, S.T., 2002. Continental Trace Fossils: SEPM, Short Course Notes 51, 132 pp.  
 1154 Hervé, C., 1989. *Clay Sedimentology*. Springer Verlag. Berlin, Heidelberg. 623 p.  
 1155 Hillier, S., 1995. Erosion, sedimentation and sedimentary origin of clays. In: Velde, B.  
 1156 (Ed.), *Origin and Mineralogy of Clays. Clays and the Environment*, pp 162–219.  
 1157 Springer-Verlag. Berlin, Heidelberg.  
 1158 Hofmann, R., Goudemand, N., Wasmer, M., Bucher, H., Hautmann, M., 2011. New  
 1159 trace fossil evidence for an early recovery signal in the aftermath of the end-Permian  
 1160 mass extinction. *Palaeogeography, Palaeoclimatology, Palaeoecology* 310, 216–226.  
 1161 Hofmann, R., Hautmann, M., Bucher, H., 2013. A new palaeoecological look at the  
 1162 dinwoody Formation (Lower Triassic, Western USA): Intrinsic versus extrinsic controls  
 1163 on ecosystem recovery after the end-Permian mass extinction. *Journal of Paleontology*  
 1164 87, 854–880.

1165 Hong, H. L., Li, Z., Xue, H. J., Zhu, Y. H., Zhang, K. X., Xiang, S. Y., 2007. Oligocene  
 1166 clay mineralogy of the Linxia Basin: Evidence of paleoclimatic evolution subsequent to  
 1167 the initial-stage uplift of the Tibetan plateau. *Clays and Clay Minerals* 55, 491–503.  
 1168  
 1169 Joachimski, M. M., Lai, X., Shen, S., Jian, H., Lou, G., Chen, B., Chen, J., Sun, Y.,  
 1170 2012. Climate warming in the latest Permian and Permian-Triassic mass extinction.  
 1171 *Geology* 40, 195–198.  
 1172  
 1173 Jones, S. J., Frostick, L. E., Astin, T. R. 2001. Braided stream and flood plain  
 1174 architecture: the Rio Vero Formation, Spanish Pyrenees. *Sedimentary Geology* 139,  
 1175 229–260.  
 1176  
 1177 Kearsey, T., Twitchett, R. J., Price, G. D., Grimes, S. T., 2009. Isotope excursions and  
 1178 palaeotemperature estimates from the Permian/Triassic boundary in the Southern Alps  
 1179 (Italy). *Palaeogeography, Palaeoclimatology, Palaeoecology* 279, 29–40.  
 1180  
 1181 Kider, D. L., Worsley, T. R., 2004. Causes and consequences of extreme Permo-  
 1182 Triassic warming to globally equable climate and relation to the Permo-Triassic  
 1183 extinction and recovery. *Palaeogeography, Palaeoclimatology, Palaeoecology* 203, 207–  
 1184 237.  
 1185  
 1186 Kiehl, J. T., Shields, C. A., 2005. Climate simulation of the latest Permian: implications  
 1187 for mass extinction. *Geology* 33, 757–760.  
 1188

1189 Kiehl, J. T, Shields, C. A., 2005. Climate simulation of the latest Permian: Implication  
 1190 for mass extinction. *Geology* 33, 757–760.  
 1191

1192 Klein, H., Voigt, S., Hminna, A., Saber, H., Schneider, J., Hmich, D., 2010. Early  
 1193 Triassic Archosaur-Dominated Footprint Assemblage from the Argana Basin (Western  
 1194 High Atlas, Morocco). *Ichnos* 17, 215–227.  
 1195

1196 Kozur, H. W., Weems, R. E., 2011. Detailed correlation and age of continental late  
 1197 Changhsingian and earliest Triassic beds: Implications for the role of the Siberia trap in  
 1198 the Permian-Triassic biotic crisis. *Palaeogeography, Palaeoclimatology, Palaeoecology*  
 1199 308, 22–40.  
 1200

1201 Kozur, H. W., Bachmann, G. H., 2008. Updated correlation of the Germanic Triassic  
 1202 with the Tethyan scale and assigned numeric ages. *Ber. Geol. Bundesanst.* 76, 1–6.  
 1203

1204 Kustatscher, E., Franz, M., Heunisch, C., Reich, M., Wappler, T., 2014. Floodplain  
 1205 habitats of braided river systems: depositional environment, flora and fauna of the  
 1206 Solling Formation (Buntsandstein, Early Triassic) from Bremke and Fürstenberg  
 1207 (Germany). *Palaeodivers. Palaeoenviron.* 94, 237–270.  
 1208

1209 Kutzbach, J.E., Gallimore, R.G., 1989. Pangean climates: megamonsoon of the  
 1210 megacontinent. *Journal of Geophysical Research* 94, 3341–3357.  
 1211

1212 Loope, D.B., 1988. Rhizoliths and ancient aeolianites. *Sedimentary Geology* 56, 301–  
 1213 314.

1214

1215 López-Gómez, J., Arche, A., 1993. Architecture of the Cañizar fluvial sheet sandstones.

1216 In: Marzo, M., Puigdefábregas, C. (Eds.), Alluvial Sedimentation. Spec. Publ. Int. Ass.

1217 Sedimentol. 17, 363–381. Blackwell Scientific Publications, Oxford.

1218

1219 López-Gómez, J., Arche, A., De la Horra, R., Galán-Abellán, B., Barrenechea, J.F.,

1220 2011. Permian-Triassic continental rocks of the SE Iberian Ranges: architecture,

1221 tectonics and geochemical characteristics in the context of a rift basin. In: Arenas, C.,

1222 Pomar, L., Colombo, F. (Eds.). Post-Meeting Field Trips Guidebooks. 28<sup>Th</sup> IAS

1223 Meeting, Zaragoza. Sociedad Geológica de España. Geo-Guías 8, 11–43.

1224

1225 López-Gómez, J., Galán-Abellán, B., De la Horra, R., Barrenechea, J. F., Arche, A.,

1226 Bourquin, S., Marzo, M., Durand, M., 2012. Sedimentary evolution of the continental

1227 Early-Middle Triassic Cañizar Formation (Central Spain): implications for life recovery

1228 after the Permian-Triassic crisis. Sedimentary Geology 249–250, 26–44.

1229

1230 Machette, M. N., 1985. Calcic soils of the southwestern United States. In: Weide, D. L.

1231 (Ed.), Soils and Quaternary Geology of the Southwestern United States. Spec. Pap.

1232 Geol. Soc. Amer. 203, 10–21.

1233 Mader, D., 1990. Palaeocology of the flora in Buntsandstein and Keuper in the Triassic

1234 of Middle Europe. G. Fischer Verlag, Stuttgart, New York. 1582 p.

1235 Martínez-Catalán, J. R., 2011. Are the oroclines of the Variscan belt related to late

1236 Variscan strike-slip tectonics? Terra Nova 23, 241–247.

- 1237 Martín-Martín, J. D., Gómez-Gras, D., Sanfeliu, T., Thiry, M., Ruiz-Cruz, M. D.,  
1238 Franco, F., 2007. Extensive dicitization of the Permo-Triassic fluvial sandstones from  
1239 the eastern Iberian Range, Spain. *Clays and Clay Minerals* 55 (5), 481–490.  
1240
- 1241 Marzo, M., 1980. El Buntsandstein de los Catalánides: Estratigrafía y procesos de  
1242 sedimentación. Ph.D Thesis. Barcelona University. Unpublished.
- 1243 Marzo, M., 1986. Secuencias fluvio-eólicas en el Buntsandstein del Macizo de Garraf  
1244 (provincia de Barcelona). *Cuad. Geol. Iber.* 10, 207–233.  
1245
- 1246 Marzo, M., Anadón, P., 1977. Evolución y características sedimentológicas de las facies  
1247 fluviales basales del Buntsandstein de Olesa de Montserrat (provincia de Barcelona).  
1248 Cuadernos de Geología Ibérica 4, 211–222.  
1249
- 1250 Marzo, M., Esteban, M., Pomar, L., 1974. Presencia de caliche fósil en el Buntsandstein  
1251 del valle del Congost (Provincia de Barcelona). *Acta Geológica Hispánica* IX (2), 33–  
1252 36.
- 1253 McKie, T., Williams, B., 2009. Triassic palaeogeography and fluvial dispersal across  
1254 the northwest European Basins. *Geological Journal* 44, 711–741.
- 1255 Miall, A.D., 1992. Alluvial Deposits. In: Walker, R.G., James, N.P. (Eds.), *Facies*  
1256 *Models: response to sea level change*. Geological Association of Canada. St. John's,  
1257 Newfoundland, pp. 119–142
- 1258 Miall, A.D., 1996. *The Geology of Fluvial Deposits. Sedimentary Facies, Basin*  
1259 *Analysis and Petroleum Geology*. Springer-Verlag. Berlin. 582 p.

1260 Middleton, G. V., Trujillo, A., 1984. Sedimentology and depositional setting of the  
 1261 Upper Proterozoic Scanlan Conglomerate, Central Arizona. In: Koster, E. H., Steel, R.  
 1262 (Eds.), Sedimentology of gravels and conglomerates. Mem. Can. Soc. Petrol. Geol. 10,  
 1263 189–201.

1264 Montañez, I., Tabor, N., Niemeier, D., DiMichele, W., Frank, T. D., Fielding, C. R.,  
 1265 Isbell, J., Birgenheier, L.P., Rygel, M.C., 2007. CO<sub>2</sub>-Forced climate and vegetation  
 1266 instability during Late Paleozoic deglaciation. Science 315, 87–89.

1267

1268 Mountney, N. P., 2006. Eolian Facies Models. In: Posamentier, H. W., Walker, R. G.  
 1269 (Eds.), Facies Models Revisited. SEPM Special Publication 84, pp. 19–83.

1270

1271 Mountney, N. P., 2012. A stratigraphic model to account for complexity in aeolian dune  
 1272 and interdune successions. Sedimentology 59, 964–989.

1273

1274 Muttoni, G., Gaetani, M., Kent, D.V., Sciunnach, D., Angiolini, L., Berra, F., Garzanti,  
 1275 E., Mattei, M., Zanchi, A., 2009. Opening of Neo-Tethys Ocean and Pangea B to  
 1276 Pangea A transformation during the Permian. GeoArabia 14 (4), 17–48.

1277

1278 Nemec, W., Postma, G., 1993. Quaternary alluvial fans in Southeastern Creta:  
 1279 Sedimentation, Processes and geomorphic evolution. In: Marzo, M., Puigdefábregas, C.  
 1280 (Eds.), Alluvial Sedimentation. Int. Assoc. Sedimentol. Spec. Publ. 17, 235–276.

1281

1282 Nikishin, A. M., Ziegler, P. A., Abbott, D., Brunet, M.-F., Cloetingh, S., 2002. Permo-  
 1283 Triassic intraplate magmatism and rifting in Eurasia: implications for mantle plumes  
 1284 and mantle dynamics. *Tectonophysics* 351, 3–39.

1285

1286 Ogg, J.G., Huang, C., Hinnov, L., 2014. Triassic timescale status: A brief overview.  
 1287 *Albertiana* 41, 3–30.

1288

1289 Oyarzun, R., Doblas, M., López-Ruiz, J., Cebriá, J.M., Youbi, N., 1999. Tectonically-  
 1290 induced icehouse-hothouse climate oscillations during the transition from the Variscan  
 1291 to the Alpine cycle (Carboniferous to Triassic). *Bulletin de la Société Géologique de*  
 1292 *France* 170, 3–11.

1293

1294 Payne, J. L., Lehrmann, D. J., Wei, J., Orchard, M. J., Scharg, D. P., Knoll, A. H., 2004.  
 1295 Large perturbations of the carbon cycle during recovery from the end-Permian  
 1296 extinction. *Science* 305, 506–509.

1297 Payne, J. L., Kump, L. R., 2007. Evidence for recurrent Early Triassic massive  
 1298 volcanism from quantitative interpretation of carbon isotope fluctuations. *Earth and*  
 1299 *Planetary Science Letters* 256, 264–277.

1300

1301 Pecorini G., 1962. Nuove osservazioni sul Permico della Nurra (Sardegna nord-  
 1302 occidentale). *Atti Acc. Naz. Lincei, Rend. Cl. fis. mat. e nat.* 8 (32) 377–380.

1303

1304 Pittau, P., Del Rio M., 2002. Palynofloral biostratigraphy of the Permian and Triassic  
 1305 sequences of Sardinia. *Rend. Soc. Paleont. It.* 1, 93–109.



1306

1307 Posenato, R., 2008. Patterns of bivalve biodiversity from Early to Middle Triassic in the  
1308 Southern Alps (Italy): Regional vs. global events. *Palaeogeography, Palaeoclimatology,*  
1309 *Palaeoecology* 261, 145–159.

1310

1311 Preto, N., Kustatscher, E., Wignall, P.B., 2010. Triassic climates – State of the art and  
1312 perspectives. *Palaeogeography, Palaeoclimatology, Palaeoecology* 290, 1–10.

1313

1314 Ramos, A., 1995. Transition from alluvial to coastal deposits (Permian-Triassic) on the  
1315 Island of Mallorca, western Mediterranean. *Geological Magazine* 132, 435–447.

1316

1317 Ramos, A., Doubinger, J., 1989. Premières datations palynologiques dans le faciès  
1318 Buntsandstein de l'Ile de Majorque (Balears, Espagne). *C. R. Acad. Sci., Paris, Ser. 2*  
1319 (309), 1089–1094.

1320

1321 Retallack, G., Sheldon, N. D., Carr, P. F., Fanning, M., Thompson, C. A., Williams, M.  
1322 L., Jones, B. G., Hutton, A., 2011. Multiple Early Triassic greenhouse crises impeded  
1323 recovery from Late Permian mass extinction. *Palaeogeography, Palaeoclimatology,*  
1324 *Palaeoecology* 308, 233–251.

1325

1326 Retallack, G. J., 1977. *A Colour Guide to Paleosols*. John Wiley and Sons, Chichester,  
1327 England, 175 pp.

1328 Retallack, G.J., 1988. Field recognition of paleosols. In: Reinhardt, J., Sigleo, W. R.  
1329 (Eds), *Paleosols and Applications*. *Spec. Pap. Geol. Soc. Amer*, 216, 1–21.

1330 Retallack, G. J., 2005. Pedogenic carbonate proxies for amount and seasonality of  
 1331 precipitation in paleosols. *Geol. Soc. Am.* 33, 333–336.

1332 Righi, D., Meunier, A., 1995. Origin of Clays by Rock Weathering and Soil Formation.  
 1333 in: Velde, B. (Ed.), *Origin and Mineralogy of Clays*. Springer-Verlag Berlin-  
 1334 Heidelberg, 43–161.

1335

1336 Rodríguez-López, J., Meléndez, M. N., De Boer, P., Soria, A. R., 2011. Control on  
 1337 marine erg-margin cycle variability: aeolian-marine interaction in the mid-Cretaceous  
 1338 Iberian Desert System, Spain. *Sedimentology* 59 (2), 466–501.

1339

1340 Röhling, H. G., 1991. A lithostratigraphic subdivision of the Lower Triassic in the  
 1341 Northwest German Lowlands and the German sector of the North Sea, based on  
 1342 gamma-ray and sonic logs. *Geologisches Jahrbuch A* 119, 3–24.

1343

1344 Romano, C., Goudemand, N., Vennemann, T.W., Ware, D., Schneebeil-Hermann, E.,  
 1345 Hochuli, P. A., Binkmann, W., Bucher, H., 2013. Climatic and biotic upheavals  
 1346 following the end-permian mass extinction. *Nature Geoscience* 6, 57–60.

1347

1348 Ronchi, A., Gretter, N., López-Gómez, J., Arche, A., De la Horra, R., Barrenechea, J.,  
 1349 Lago, M., 2014. Facies analysis and evolution of the Permian and Triassic volcano-  
 1350 sedimentary succession in the Eastern Pyrenees (Spain) and its regional correlation in  
 1351 the western Peri-Tethys. *Carboniferous-Permian Meeting Freiberg*, Abstract book, pp.  
 1352 20–22.

1353

1354 Roscher, M., Stordal, F., Svensen, H., 2011. The effect of global warming and  
 1355 globalcooling on the distribution of the latest Permian climate zones. *Palaeogeography,*  
 1356 *Palaeoclimatology, Palaeoecology* 309, 186–200.  
 1357  
 1358 Schmidt, M., 1937. Probleme der westmediterranen Kontinentaltrias und Versuche ihrer  
 1359 Lösung. *Association pour l'étude géologique de la Méditerranée occidentale* 4, (11), 3–  
 1360 57.  
 1361  
 1362 Self, S., Blake, S., Sharma, K., Widdowson, M., Sephton, S., 2008. Sulfur and chlorine  
 1363 in Late Cretaceous Deccan magmas and eruptive gas release. *Science* 319, 1654–1657.  
 1364  
 1365 Sellwood, B.W., Valdes, P.J., 2007. Mesozoic climates. In: Williams, M., Haywood,  
 1366 A.M., Gregory, F.J., Schmidt, D.N. (Eds.), *Deep-Time Perspectives on Climate Change:*  
 1367 *Marrying the signal from Computer Models and Biological Proxies.* The  
 1368 *Micropalaeontological Society, Special Publication.* The Geological Society, London,  
 1369 201–224.  
 1370  
 1371 Smith, R. M. H., 1995. Changing fluvial environments across the Permian-Triassic  
 1372 boundary in the Karoo Basin, South Africa and possible causes of tetrapods extinctions.  
 1373 *Palaeogeography, Palaeoclimatology, Palaeoecology* 117, 81–104.  
 1374  
 1375 Soil Survey Staff (1999): *Keys to Soil Taxonomy.* Pocahontas Press, Blackburg. 600  
 1376 pp.

- Soria, A. R., Liesa, C., Rodríguez-López, J. P., Meléndez, N., De Boer, P., Meléndez, A., 2011. An Early Triassic evolving erg system (Iberian Chain, NE Spain): Paleoclimate implications. *Terra Nova* 23, 76–84.
- Stampfli, G. M., Borel, G. D., 2002. A plate tectonic model for the Paleozoic and Mesozoic constrained by dynamic plate boundaries and restored synthetic oceanic isochrones. *Earth and Planetary Science Letters* 196, 17–33.
- Stefani, M., Furin, S., Gianolla, P., 2010. The changing climate framework and depositional dynamics of Triassic carbonate platforms from the Dolomites. *Palaeogeography, Palaeoclimatology, Palaeoecology* 290, 43–57.
- Sun, Y., Joachimski, M., Wignall, P. B., Yan, C., Chen, Y., Jiang, H., Wang, L., Lai, X., 2012. Lathally hot temperatures during the Early Triassic greenhouse. *Science* 338, 336–370.
- Takahashi S., Yamasaki S., Ogawa K., Kaiho K., Tsuchiya N. (in press). Redox conditions in the end-Early Triassic Panthalassa. *Palaeogeography, Palaeoclimatology, Palaeoecology*. DOI: doi: 10.1016/j.palaeo.2015.04.018
- Tourani, A., Benaouiss, N., Gand, G., Bourquin, S., Jalil, N-E., Broutin, J., Battail, B., Germain, D., Khaldoune, F., Sebban, S., Steyer, J-S., Vacant, R., 2010. Evidence of an Early Triassic age (Olenekian) in Argana Basin (High Atlas, Morocco) based on new chirotherioid traces. *Comptes Rendus Palevol* 9, 201–208.

1402 Twitchett, R. J., 2007. Climate change across the Permian/Triassic boundary. In:  
 1403 Williams, M., Haywood, A., Gregory, F., Schmidt, D. N. (Eds.), Deep-Time  
 1404 Perspectives on Climate Change: Marrying the Signal from Computer Models and  
 1405 Biological Proxies. The Micropaleontological Society, Special Publications. The  
 1406 Geological Society, London, pp. 191–200.

1407

1408 Twitchett, R.J., 2006. The palaeoclimatology, palaeoecology and palaeoenvironmental  
 1409 analysis of mass extinction events. *Palaeogeography, Palaeoclimatology, Palaeoecology*  
 1410 232, 290–213.

1411

1412 Tyrrell, S., Haughton, P. B. W., Souders, A.K., Daly, J. S., Shanonn, P. M., 2012.  
 1413 Large-scale, linked drainage systems in the NW European Triassic. Insights from the Pb  
 1414 isotopic composition of detrital K-feldspar. *Journal of the Geological Society, London*  
 1415 169, 279–295.

1416 Velde, B., Meunier, A. 2008. *The Origin of Clay Minerals in Soils and Weathered*  
 1417 *Rocks*. Springer-Verlag, Berlin-Heidelberg. 406 pp.

1418

1419 Van Wees, J-D., Arche, A., Beijdorff, C. G., López-Gómez, J., Cloetingh, S.A.P.L.,  
 1420 1998. Temporal and spatial variations in tectonic subsidence in the Iberian Basin  
 1421 (eastern Spain): inferences from automated forward modelling of high-resolution  
 1422 stratigraphy (Permian-Mesozoic). *Tectonophysics* 300, 285–310.

1423

1424 Vargas, H., Gaspar-Escribano, J., López-Gómez, J., van Wees, J-D., Cloetingh, S., De  
 1425 la Horra, R., Arche, A., 2009. A comparison of the Iberian and Ebro Basins during the

1426 Permian and Triassic, eastern Spain: A quantitative subsidence modelling approach.  
 1427 Tectonophysics 474, 160–183.

1428

1429 Wand, C., Hong, H., Li, Z., Yin, K., Xie, J., Liang, G., Song, B., Zhang, K., 2013. The  
 1430 Eocene-Oligocene climate transition in the Tarim Basin, Northwest China: Evidence  
 1431 from clay mineralogy. *Applied Clay Science* 74, 10–19.

1432 Weil, A. B., Van der Voo, R., Van der Pluijm, B., 2001. Oroclinal bending and  
 1433 evidence against the Pangea megashear: the Cantabria-Asturias arc (northern Spain).  
 1434 *Geology* 29 (11), 991–994.

1435

1436 Wignall, P. B., 2007. The end-Permian mass extinction-how bad did it get? *Geobiology*  
 1437 5, 303–309.

1438

1439 Wignall, P.B., 2001. Large igneous provinces and mass extinctions. *Earth-Science*  
 1440 *Review* 53, 1–33.

1441

1442 Willis, B. J., 1989. Palaeochannel reconstruction from point bar deposits: a three-  
 1443 dimensional perspective. *Sedimentology* 36, 757–766.

1444

1445 Willis, B. J., Behrensmeyer, A. K., 1994. Architecture of Miocene overbank deposits in  
 1446 northern Pakistan. *Jour. Sediment. Res.* 64, 60–67.

1447

1448 Yakimenko, E., Targul'yan, V., Chumakov, N., Arefev, M., Inozemtsev, S., 2000.  
 1449 Paleosols in Upper Permian sedimentary rocks, Sukhona River (Severnaya Dvina  
 1450 basin). *Lithology and Mineral Resources* 35, 331–344.  
 1451  
 1452 Yin, H., Song, H., 2013. Mass extinction and Pangea integration during the Paleozoic-  
 1453 Mesozoic transition. *Science China: Earth Sciences* 56 (11), 1791–1803.  
 1454  
 1455 Ziegler, P. A., 1988. Post-Hercynian plate reorganization in the Tethys and Arctic-North  
 1456 Atlantic domains. In: Manspeizer, W. (Ed.), *Triassic-Jurassic Rifting. Developments in*  
 1457 *Geotectonics* 22. Elsevier, Amsterdam, pp 711–755.  
 1458 Ziegler, P.A., Stampfli, G.M., 2001. Late Paleozoic-Early Mesozoic plate boundary  
 1459 reorganization: Collapse of the Variscan Orogen and opening of the Neotethys. *Nature*  
 1460 *Bresciana. Ann. Mus. Civ. Sc. Nat. Bresc.* 25, 17–34.  
 1461  
 1462  
 1463  
 1464  
 1465  
 1466  
 1467  
 1468  
 1469  
 1470  
 1471

## Figure captions

Fig. 1. Early Triassic global map showing the configuration of the continents (modified from Golonka and Ford, 2000; Yin and Song, 2013). The amplified area corresponds to the Iberian peninsula and the present-day basin and ranges: 1- Pyrenean Ranges, 2- Catalan Ranges, 3- Ebro Basin, 4- Duero Basin, 5 Iberian Ranges, 6- Tagus Basin, 7- Guadalquivir Basin, 8- Betic Ranges, 9- Iberian Massif, 10- Balearic Islands.

Fig. 2. Lithostratigraphic scheme of the Middle Permian – Middle Triassic units of the studied areas and their comparison with coeval units of NE Sardinia and Minorca. Numbers 1 to 12 represent sections cited in the text: 1- Río Mayor, 2- Gátova, 3- Cedrillas-Corbalán, 4- Torre de Las Arcas - Peñarroyas, 5- Benicassim, 6- Novés, 7- Castellar d'Hug, 8- San Gregori, 9: Cervelló, 10- El Brull-Figaró, 11- Cala Pilar, 12- Cala Viola. Their geographical location are indicated down to the right in the figure.

Fig. 3. a) The Cañizar Fm. in S. Iberian Ranges. Lines represent major boundaries surfaces (MBS) and separate subunits (A to F). The lower contact is an unconformity that separates the Triassic to the Permian (Alcotas Fm.) (Photograph modified from López-Gómez et al., 2012). b) The Eslida Fm. in the E Iberian Ranges.

Fig. 4. Main characteristics and references of the lithological units of the studied areas.

Fig. 5. Studied Lower-Middle Triassic sections and their main sedimentary and paleontological characteristics of the S. Iberian Ranges, E. Pyrenees and Catalan Ranges. Their geographical locations are indicated in figure 2. Description of the



architectural elements is shown in figure 7. C1 to C6 and Ems-3 to Ems-6 represents subunits of the Cañizar Fm. and Eslida Fm. respectively.

Fig. 6. Description, interpretation and codes of the main and secondary fluvial and aeolian facies.

Fig. 7. Fluvial and aeolian architectural elements showing their codes, facies associations, hierarchy and vertical stacking patterns, and selected references.

Fig. 8. Pictures of the different described architectural elements: a) element GB in the Garraf Upper Conglomerates Unit (GUC), Catalan Ranges; b) element GM in the Prades Upper Conglomerates Unit (PUC), Catalan Ranges; c) SB and CH elements in the Cañizar Fm. (CS), Iberian Ranges; d) E1 element in Prades Lower Sandstone Unit (PLS), Catalan Ranges; e) E2 and E3 elements in Prades Lower Sandstone (PLS), Catalan Ranges; f) FF element in Figaró Sandstones and Mudstones (FSM), Catalan Ranges; f) GB element in the lowermost part of the "Buntsandstein" deposits of the Noves section, Pyrenean Ranges; h) E1 element in the lower Buntsandstein of the Noves section, Pyrenean Ranges. See figure 5 for the location of these units and sections.

Fig. 9. Sketches of 3D evolution of three selected stages of the Buntsandstein of the Iberian Ranges showing alluvial evolution and macroflora distribution (modified from Borruel-Abadía et al., 2014).

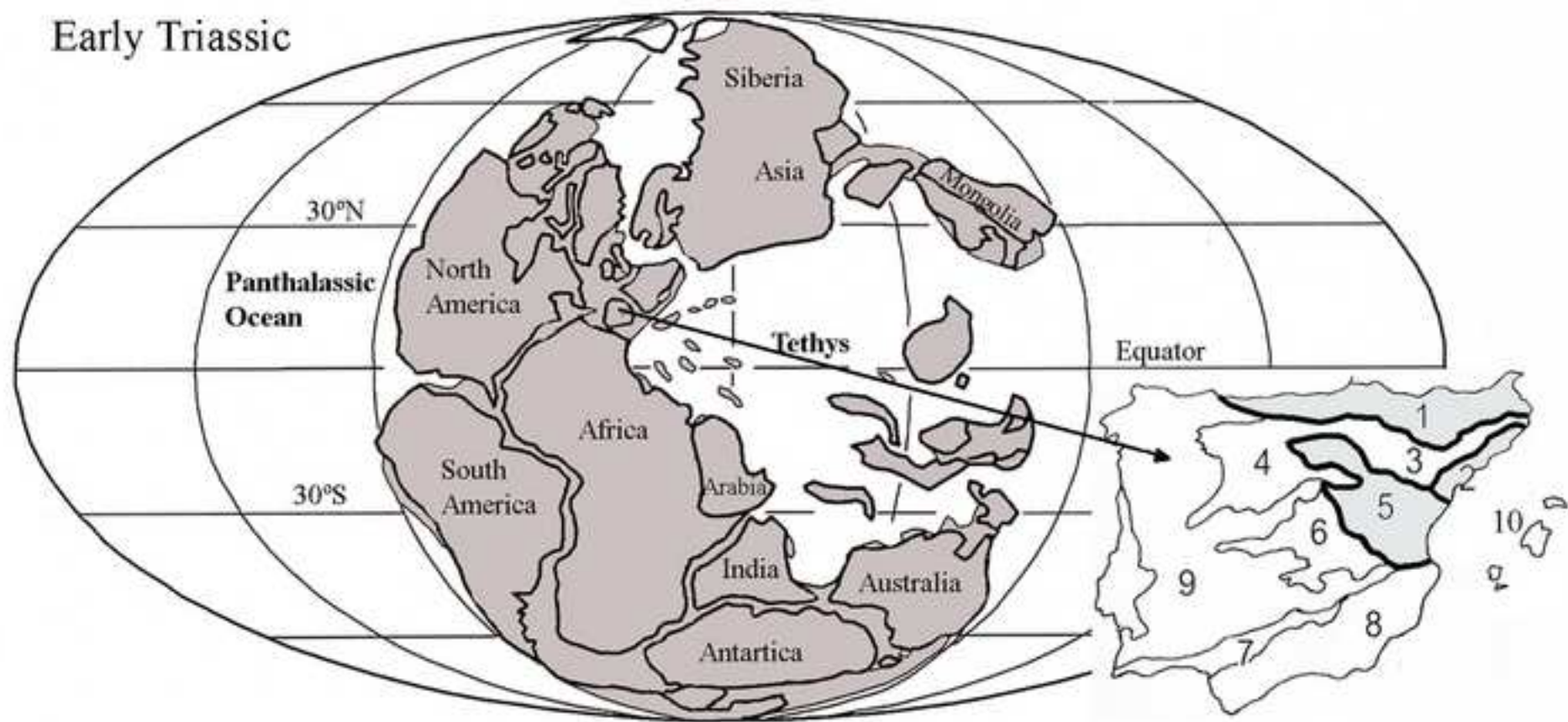
Fig. 10. Specimens of macroflora from the Eslida Fm. in the Iberian Ranges. a: *Pleuromeia sternbergii* (Münster) Corda ex Giebe, 1953; b: Sphenophytes, most likely *Equisetitesmougeotii* Brongniart 1828; c: *Pelourdea vogesiaca* (Schimper et Mougeot) Seaward 1917; d: *Albertia latifolia* Schimper et Mougeot 1944. Scale bar: 1 cm.

Fig. 11. A) Dispersed carbonate nodules are circled in the subsurface horizon of the Gat-A pedotype. Black arrows are pointing to small green root traces. B) Calcareous, rooted, and endurated yellow B horizons are irregularly truncated in the Pedotype Gat-B. C) Adventitious prop roots (marked in white) emanating from a main root in the Gat-C pedotype. White arrow is pointing to the top of another unmarked prop root pattern. D) Deep penetrating tap root with root apex (r) related to Gat-C paleosols. E) Drab-haloes of light green silt around root traces in the pedotype Gat-D.

Fig. 12. Synthesis of the main climate stages and their vertical alternating disposition during the Smithian to Pelsonian time – interval in the continental units (Buntsandstein) of the S. Iberian Ranges, E. Pyrenees and Catalan Ranges, and their relationship with fossil content. Sections (numbers 1 to 10) are located and named in figures 2 and 5.

Fig. 13. Early Triassic palaeogeographical reconstruction of Iberia and neighbour areas. Basins in Iberia were separated by elevated areas linked to the development of rift systems. Palaeolatitudes and sedimentary environments are partially based on Ziegler (1988), Dercourt et al. (1993), Mckie and Williams (2009), Bourquin et al. (2011) and Tyrrell et al. (2012).

Figure 1  
[Click here to download high resolution image](#)



**Figure 2**  
[Click here to download high resolution image](#)

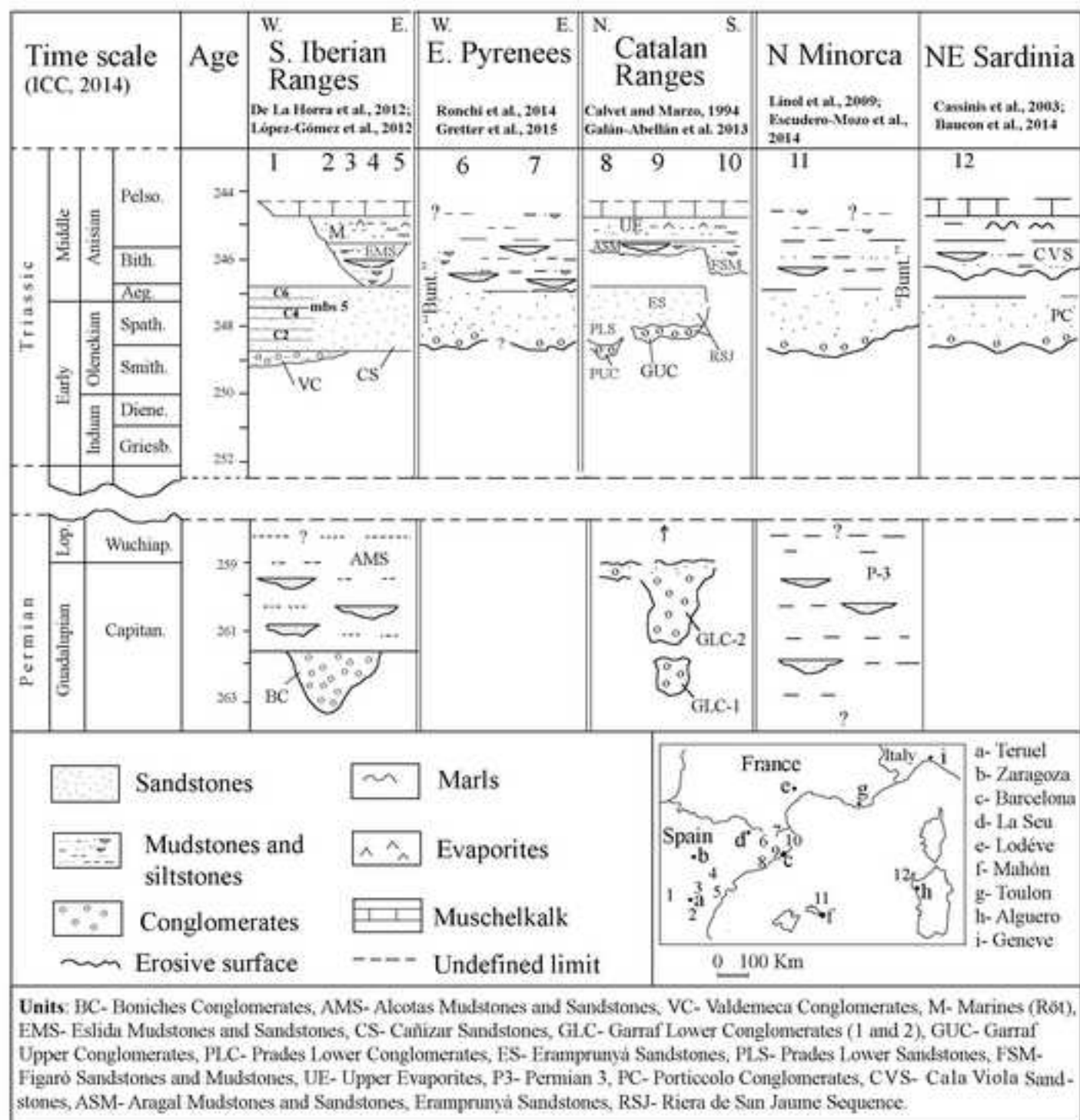




Figure 3  
[Click here to download high resolution image](#)

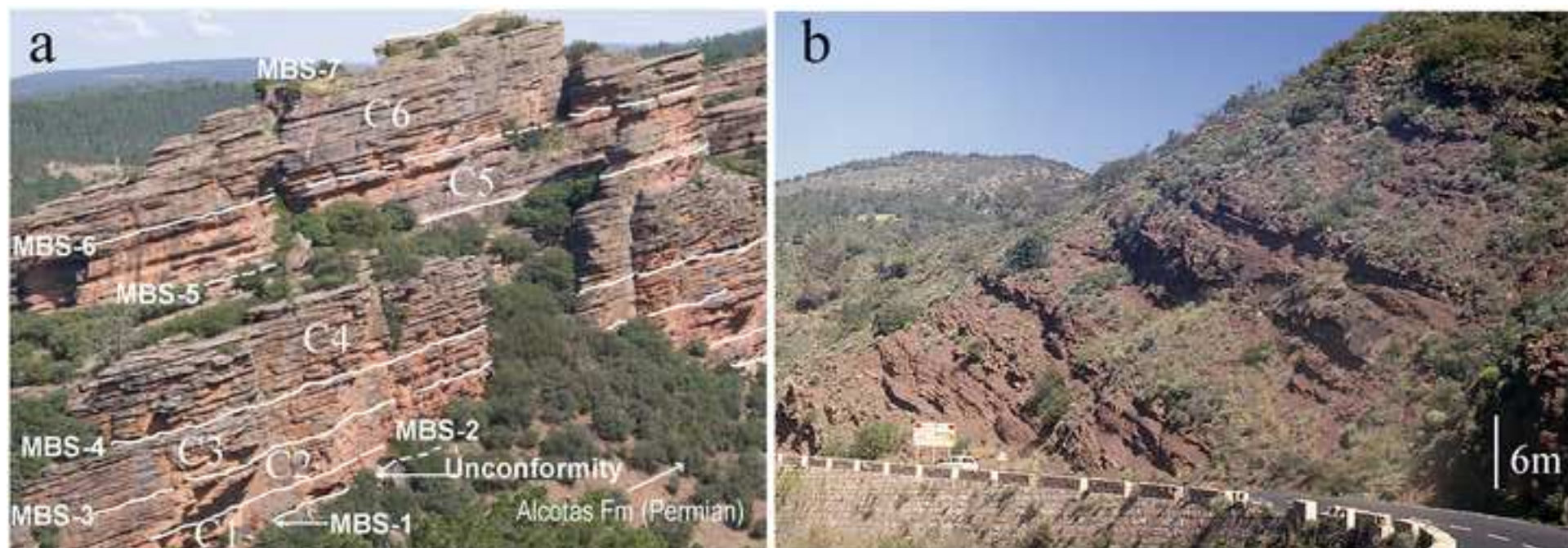


Figure 4

[Click here to download high resolution image](#)

Area	Units	Lithology	Palaeontological content and soils	Age	Interpretation	References
Iberian Ranges	Eslida Fm.	Mudstones Sandstones	Plants, footprints Pollen assemblages Soils	Aegian-Bithinian	Alluvial and punctual aeolian	López-Gómez and Arche (1993), Arche and López Gómez (1999), Borrueal et al. (2014)
	Cañizar Fm.	Sandstones	Pollen assemblage Plants, footprints	Smithian Aegian	Fluvial (braided) and aeolian	Arche and López-Gómez (2005), López-Gómez et al. (2013)
	Valdemeca Unit	Conglomerates	-----	Smithian	Fluvial (braided, unconfined), aeolian	De la Horra et al. (2005) De la Horra (2008)
Catalan Ranges	Figaró Unit	Mudstones Sandstones	Footprints, bones, Pollen assemblages Soils	Aegian-Bithinian	Fluvial (braided and meander)	Calvet and Marzo (1994) Dinarès-Turell et al. (2005)
	Prades Lower Sands. Unit	Sandstones	-----	Smithian - Aegian	Aeolian (dominating) fluvial (braided)	Marzo (1980), Calvet and Marzo (1994), Galán-Abellán et al. (2013)
	Eramprunyà	Sandstones	Plants	Smithian - Aegian	Fluvial (dominating) aeolian	Marzo (1980), Calvet and Marzo (1994), Galán-Abellán et al. (2013a)
	Garraf Upper Conglo. Unit	Conglomerates	-----	Smithian	Fluvial (dominating) aeolian	Calvet and Marzo (1994) Dinarès-Turell et al. (2005)
Pyrenees	“Upper Bunt” Unit	Mudstones Sandstones Conglomerates	Footprints, pollen assemblages	Spathian-Anisian	Fluvial (dominating) aeolian	Gisbert (1980), Ronchi et al. (2014), Grotter (2014)



Figure 5  
[Click here to download high resolution image](#)

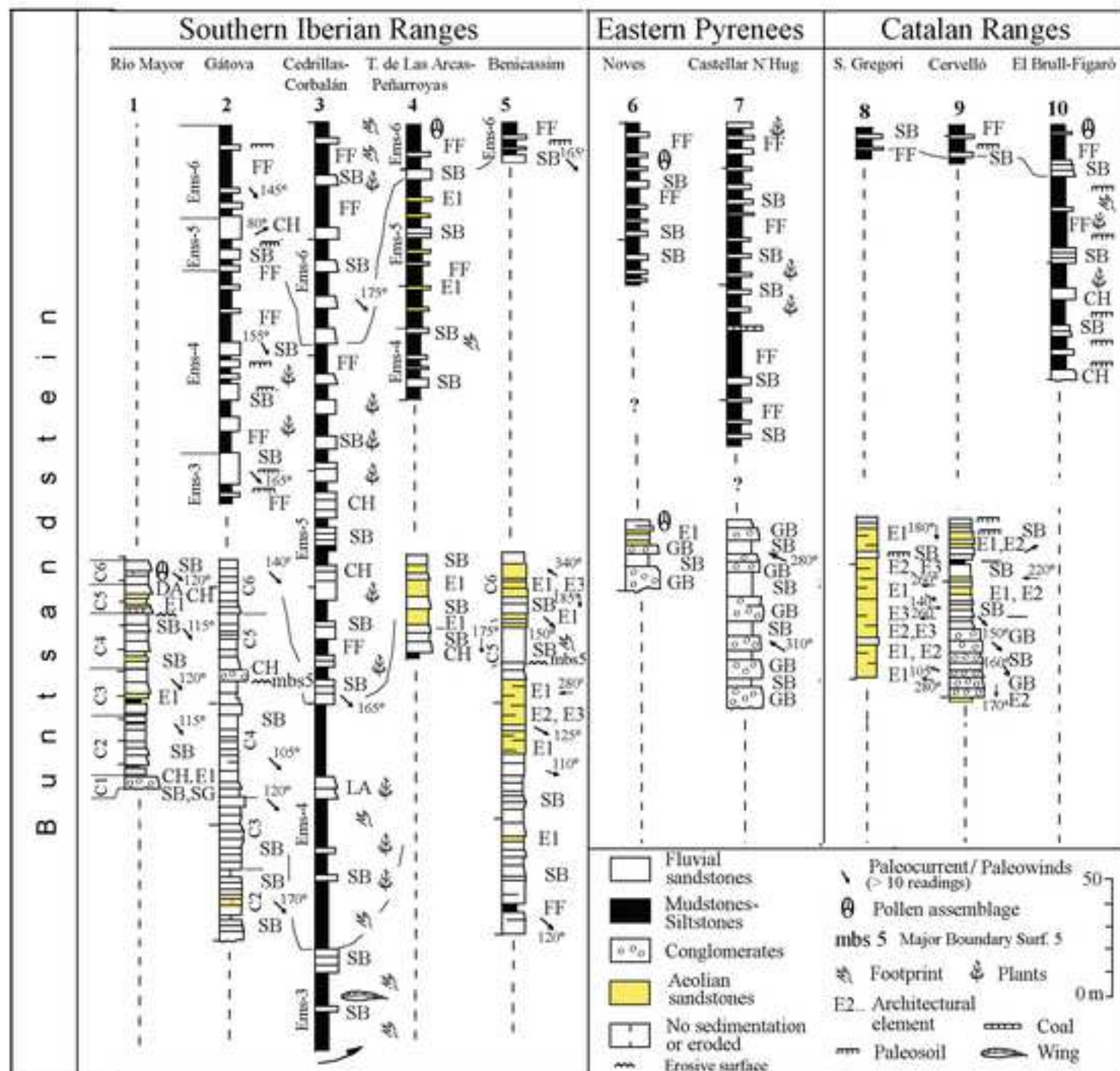


Figure 7  
[Click here to download high resolution image](#)





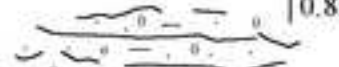
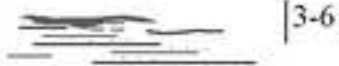




Architectural Elements		Code	Facies: Main (above) Associated (below)	Hierarchy and vertical stacking patterns	References
FLUVIAL	<b>Megaripples</b> of sandstones with erosive or planar base and basal lag.	SB	St, Sp Sh, Sr, ae4	   0.8m	Blodgett and Stanley (1980) Fielding et al. (2009) Best et al. (2003)
	<b>Channel-fill</b> complex of sandstones with defined margins and internal erosive surfaces.	CH	Sp, St Sh, Sr	   1m	Marzo and Anadón (1987) Hajek et al. (2010)
	<b>Lateral-accretion</b> deposits showing 3rd-order internal surfaces and up to 1.5 m thick.	LA	St, Sp, Sr Sh	   1m	Willis (1989) Bristow (1993)
	<b>Gravel bars</b> normally amalgamated into macroforms.	GB	Gp, Gmp, Gmt, Gt. Sp	   1.3m	Middleton and Trujillo (1984) Nemec and Postma (1993)
	<b>Unconfined or semiconfined clast bodies.</b> Beds show crude-masive stratification. Sets up to 1 m thick.	GM	Gms Gmp, St	   0.8m	Nemec and Postma (1993) Jones et al. (2001)
	<b>Floodplain</b> fines with isolated sandstone bodies and paleosols.	FF	Fr Fb, Fl, Sbp	   3-6 m	Allen and Fielding (2007) Hajek and Edmonds (2014)
	<b>Crevasse splay</b> deposits prograding into floodplain.	CS	Fr, Sr Sh	   1.3m	Willis and Behrensmeier (1994) Hampton and Horton (2007)
AEOLIAN	<b>Dune.</b> They may interact with sediments of fluvial origin, and constitute sets up to 10 m thick.	E1	ae1, ae2, ae3, ae4. ad, vs, ds, rs, df, wl, pl	   3.1m	Chrintz and Clemmensen (1993) Mountney (2012)
	<b>Sandsheet.</b> They may show translent-strata, and constitute sets up to 1 m thick and few tens of meters of lateral extension	E2	ae4, ae5. ss, df, wl.	   0.4m	Rodriguez-López et al. (2011) Brookfield (1992)
	<b>Interdune.</b> They show irregular lenses of fine-grained massive sandstones of pale-brown color and occasional mottling.	E3	ae4, ae6 Sbp, Fb, Fl, dc, wl		Loope (1988) Hasiotis (2002) Mountney (2006)



Figure 6

[Click here to download high resolution image](#)

Facies Code	Description	Interpretation	Facies Code	Description	Interpretation
St	<i>Fine to coarse red-pink sandstones. Trough cross-stratification with occasional clay chips and small quartz clasts</i>	<i>Dune of sandstones with sinuous crest (3D) of linguoid type.</i>	Fr	<i>Fine grain sandstone or mudstone, massive with rootlets</i>	<i>Abandoned channel or near channel deposits.</i>
Sp	<i>Fine to medium pink sandstones Planar cross-stratification with fining-upwards tendency.</i>	<i>Dunes of sandstones with straight crest (2D) of linguoid type.</i>	Fb	<i>Red-dark mudstones or fine-grain pink sandstones with mud-cracks and/or paleosoils.</i>	<i>Abandoned channel or near channel deposits.</i>
Sh	<i>Fine to medium pink sandstones with parallel lamination and parting lineation.</i>	<i>upper-stage phase beds movements</i>	Fl	<i>Centimetre beds of fine red sandstones with current ripples into red dark mudstones.</i>	<i>Near channel overflowing.</i>
Sr	<i>Fine to medium red-pink sandstones with current ripples.</i>	<i>Low-stage phase beds movements</i>	ae1	<i>Pale yellow, medium grained, well rounded and subangular quartz grains constituting sets with cross-bedded sandstones up to 2.5 m thickness.</i>	<i>Migration of aeolian dunes by avalanching in the lee slope.</i>
Sbp	<i>Fine red-orange sandstones with vertical bioturbation and plant remains</i>	<i>Near channel overflowing</i>	ae2	<i>Laterally continuous orange units of fine-grained sandstone laminations less than 3mm thick</i>	<i>Aeolian grain flow strata related to saltation of sand-size particles over the brink of a dune.</i>
Gp	<i>Clast-supported pink to white quartz conglomerates with planar cross-stratification.</i>	<i>Two-dimensional gravel dunes</i>	ae3	<i>Yellow, fine to medium, well-rounded quartz grains. Sets with planar or trough cross-strata and inversely graded sand tongues less than 20 mm thick</i>	<i>Aeolian grain flow strata related to avalanching in the dune lee slope during dune migration.</i>
Gt	<i>Clast-supported pink to white quartz conglomerates with trough cross-stratification.</i>	<i>Three-dimensional gravel dunes</i>	ae4	<i>Yellow to salmon-pink, fine-grain and well-sorted sandstone with subhorizontal laminations up to 2 mm thick.</i>	<i>Wind ripple-laminated/translatent strata sandstone due to migration of aeolian wind ripples.</i>
Gmp	<i>Matrix-supported pink to white quartz conglomerates with planar cross-stratification</i>	<i>Two-dimensional dunes of gravels and sandstones.</i>	ae5	<i>Salmon-pink, fine grain and well-sorted horizontally laminated (10-20 mm thick) sandstone with scarce bioturbation.</i>	<i>Horizontally laminated sandstone originated during stages with high wind velocity and restricted sediment availability.</i>
Gmt	<i>Matrix-supported pink to white quartz conglomerates with trough cross-stratification</i>	<i>Three-dimensional dunes of sandstones and gravels</i>	ae6	<i>Orange fine-grained sandstone without internal structure. Mottling and rootlets may appear</i>	<i>Remnant of aeolian sediments related to alluvial overflowing area</i>
Gms	<i>Massive flat-bedding white angular/subrounded clasts. Low sandy matrix proportion or even clast supported.</i>	<i>Low-strength flow deposited from viscous, laminar or turbulent flows</i>			

**Secondary or associated facies:** rs- Reactivation surface, ss- Small erosive grooves, ad- Small avalanching deposits, df- Deflection surfaces with angular clasts, ds- Small-scale liquefaction structures, dc- Desiccation cracks, vs- Ventifacts, pl- Pinstripe lamination, wl- Wavy laminae



Figure 8  
[Click here to download high resolution image](#)





Figure 9  
[Click here to download high resolution image](#)

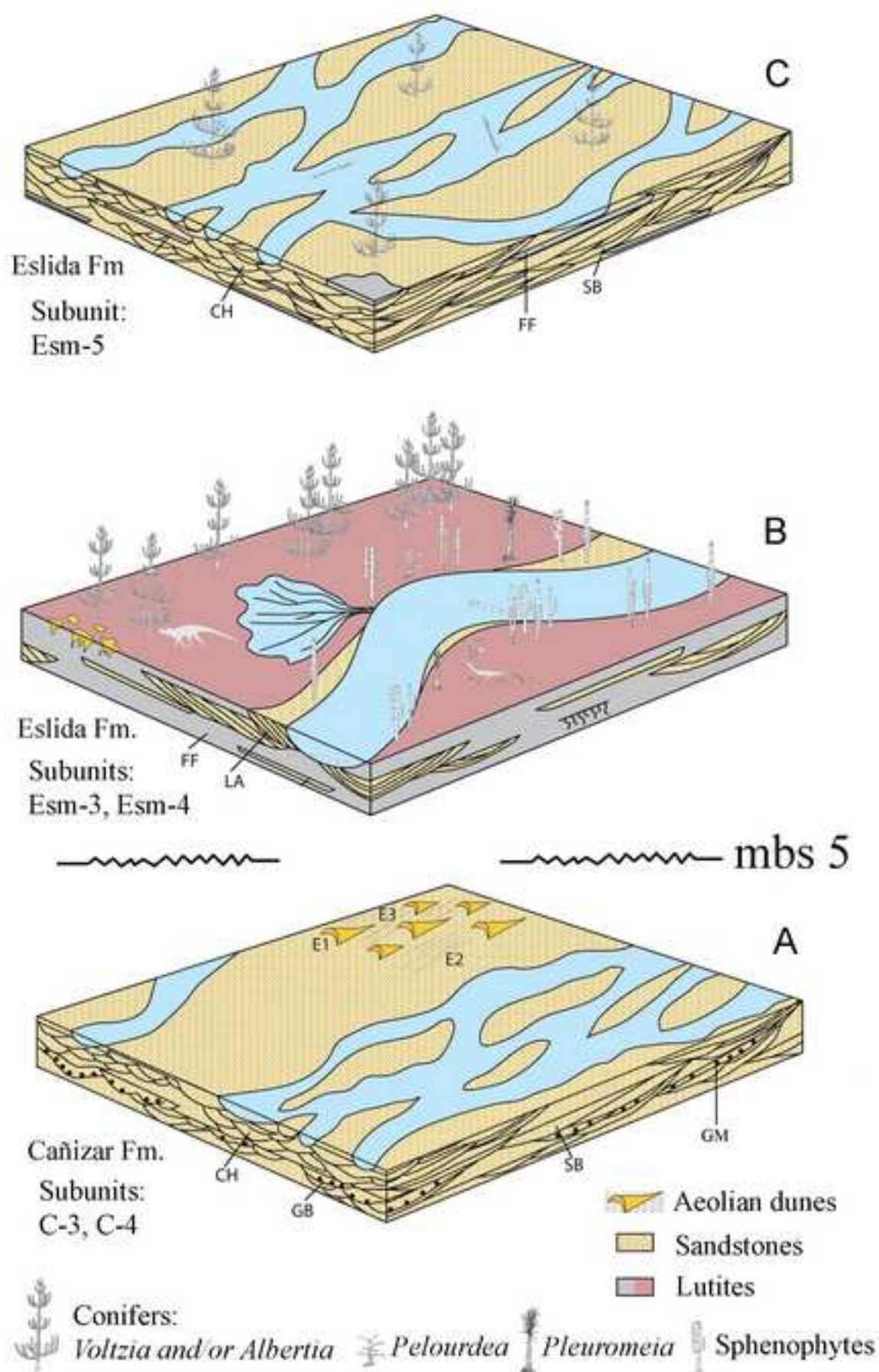




Figure 10  
[Click here to download high resolution image](#)

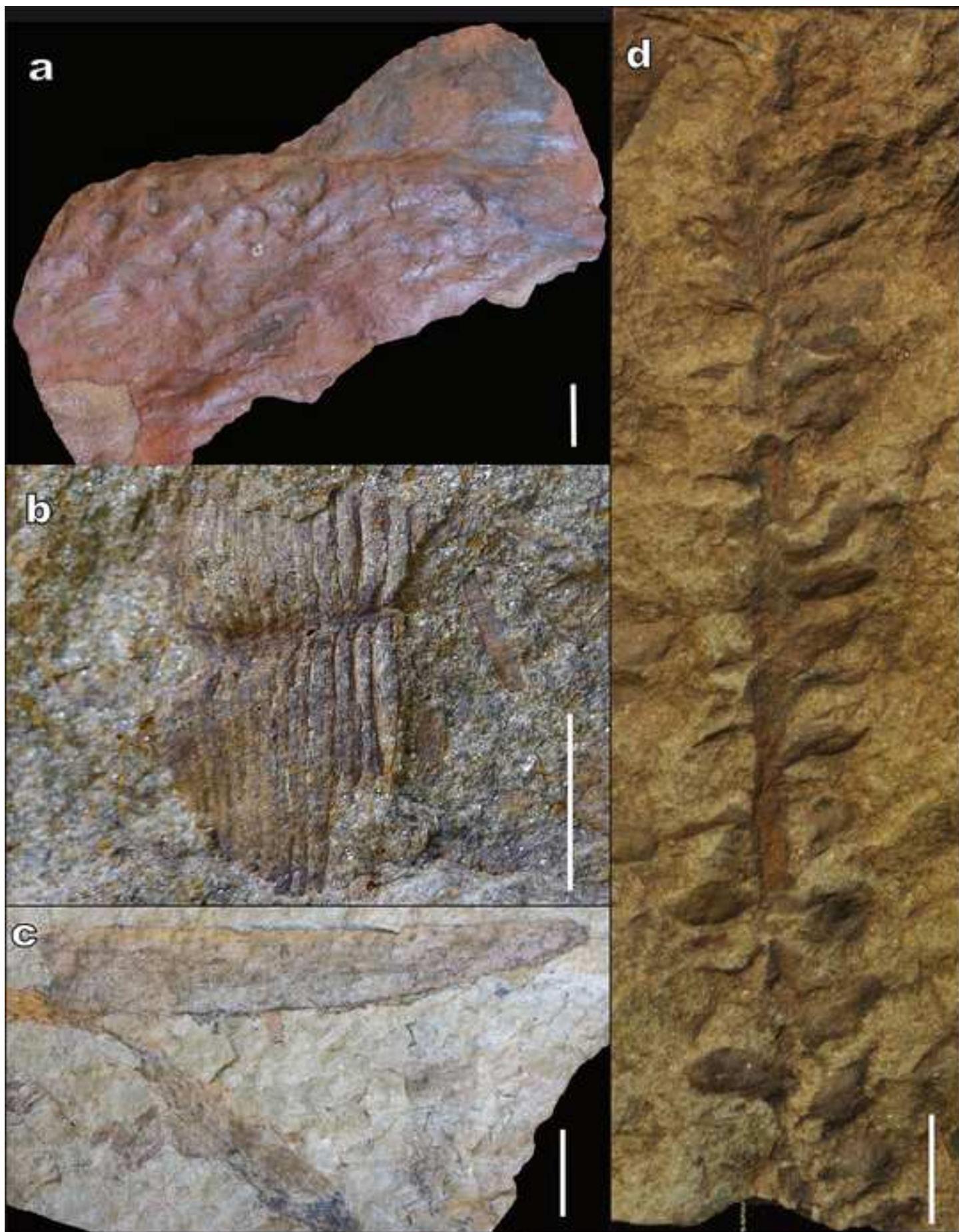




Figure 11  
[Click here to download high resolution image](#)

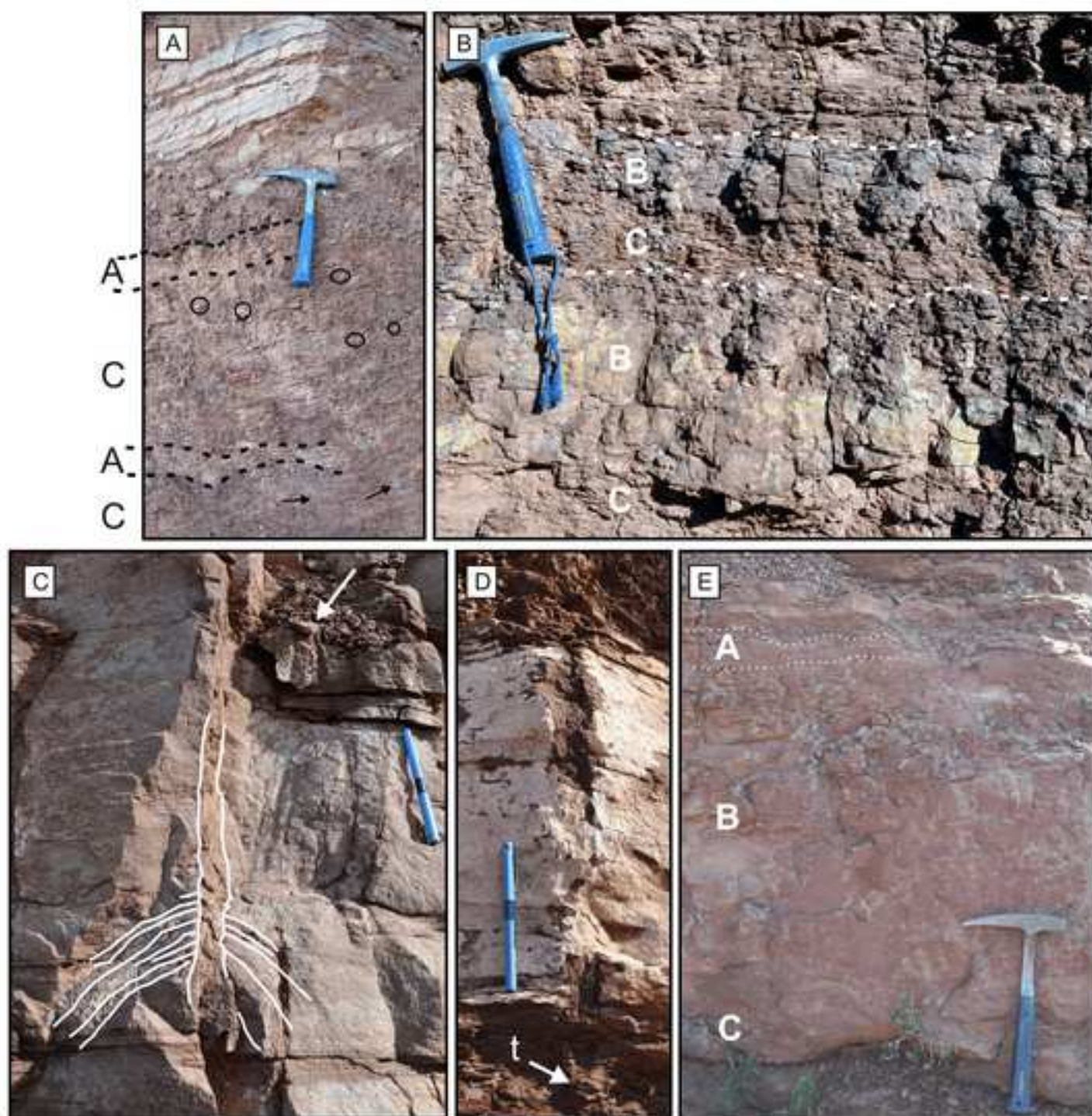


Figure 12  
[Click here to download high resolution image](#)

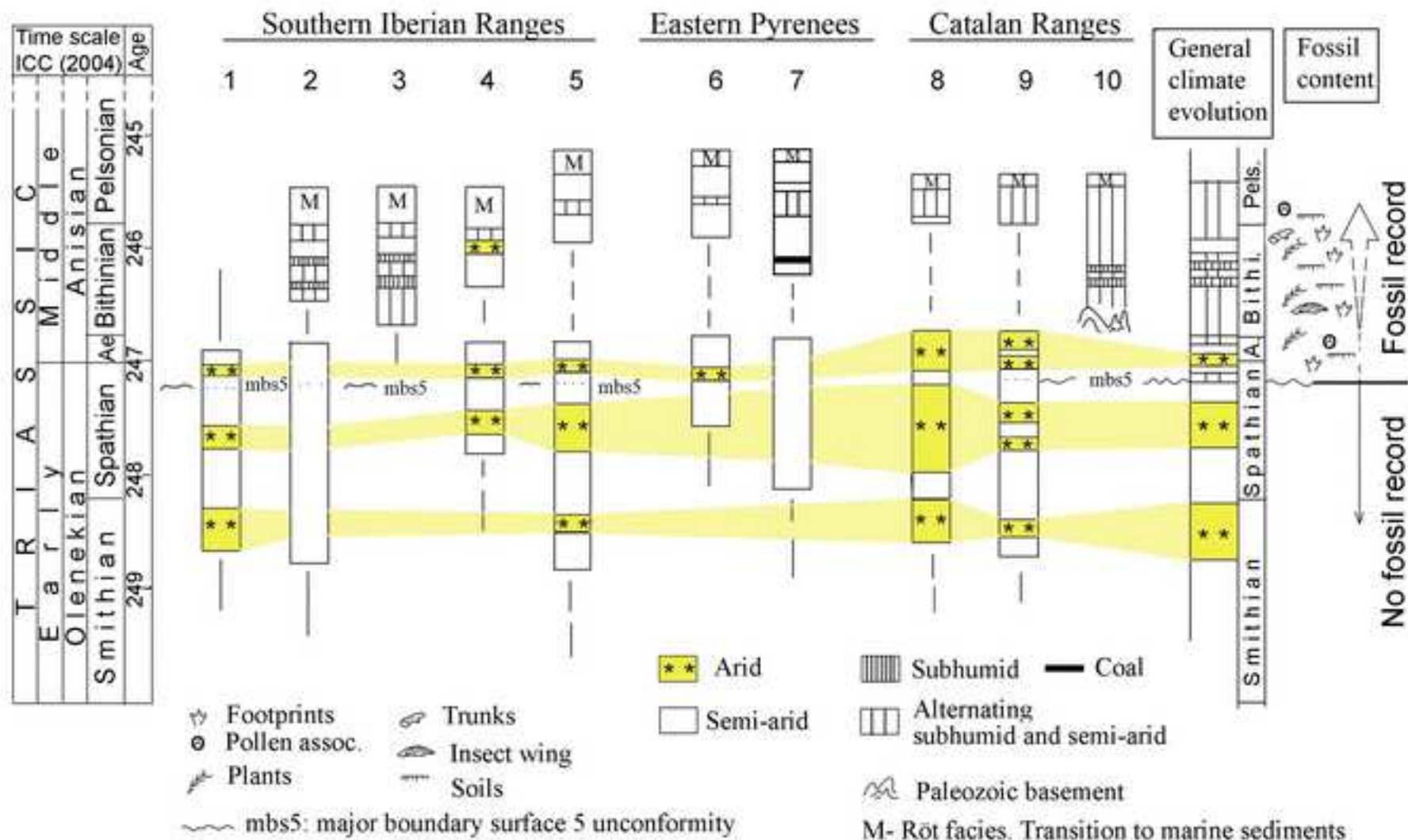

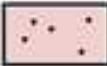


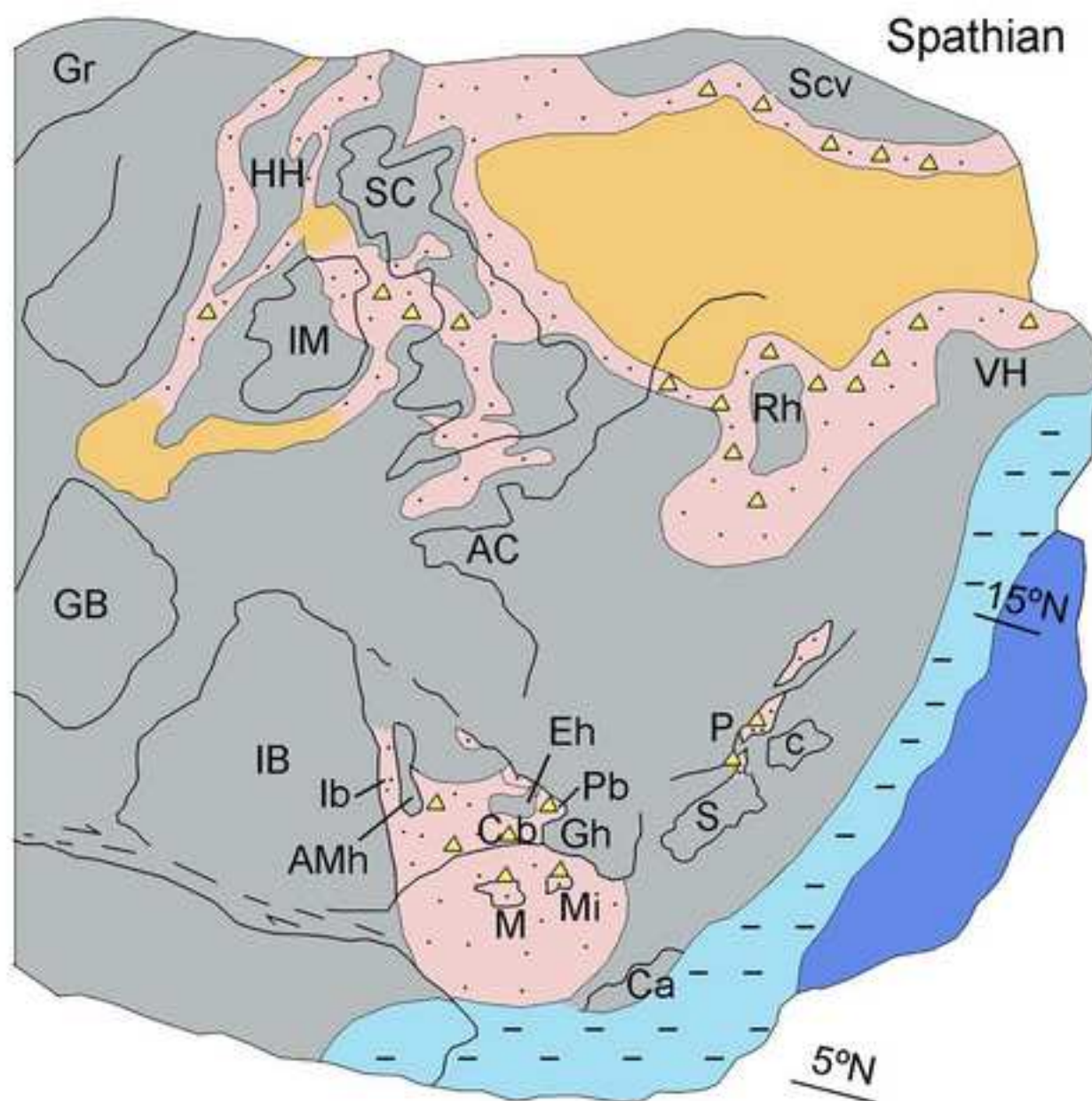


Figure 13  
[Click here to download high resolution image](#)

AC- Armorica  
 AMh- Ateca-Montalbán High  
 C- Corsica  
 Ca- Cabilia  
 Cb- Catalan basin  
 Scv- Scandinavia  
 Eh- Ebro High  
 Gb- Grand Banks  
 Gh- Girona High  
 Gr- Greenland  
 HH- Hatton High  
 IB- Iberia  
 IM- Irish Massif  
 M- Majorca  
 Mi- Minorca  
 P- Provence  
 Pb- Pyrenean basin  
 Rh- Rhenish High  
 VH- Vindicelien High

 Continental  
 Aeolian dominant  
 Fluvial

 Land masses     Playa lake     Shallow marine  
 Mainly siliciclastics     Marine carbonates



## Figure captions

Fig. 1. Early Triassic global map showing the configuration of the continents (modified from Golonka and Ford, 2000; Yin and Song, 2013). The amplified area corresponds to the Iberian peninsula and the present-day basin and ranges: 1- Pyrenean Ranges, 2- Catalan Ranges, 3- Ebro Basin, 4- Duero Basin, 5 Iberian Ranges, 6- Tagus Basin, 7- Guadalquivir Basin, 8- Betic Ranges, 9- Iberian Massif, 10- Balearic Islands.

Fig. 2. Lithostratigraphic scheme of the Middle Permian – Middle Triassic units of the studied areas and their comparison with coeval units of NE Sardinia and Minorca. Numbers 1 to 12 represent sections cited in the text: 1- Río Mayor, 2- Gátova, 3- Cedrillas-Corbalán, 4- Torre de Las Arcas - Peñarroyas, 5- Benicassim, 6- Novés, 7- Castellar d'Hug, 8- San Gregori, 9: Cervelló, 10- El Brull-Figaró, 11- Cala Pilar, 12- Cala Viola. Their geographical location are indicated down to the right in the figure.

Fig. 3. a) The Cañizar Fm. in S. Iberian Ranges. Lines represent major boundaries surfaces (MBS) and separate subunits (A to F). The lower contact is an unconformity that separates the Triassic to the Permian (Alcotas Fm.) (Photograph modified from López-Gómez et al., 2012). b) The Eslida Fm. in the E Iberian Ranges.

Fig. 4. Main characteristics and references of the lithological units of the studied areas.

Fig. 5. Studied Lower-Middle Triassic sections and their main sedimentary and paleontological characteristics of the S. Iberian Ranges, E. Pyrenees and Catalan Ranges. Their geographical locations are indicated in figure 2. Description of the



architectural elements is shown in figure 7. C1 to C6 and Ems-3 to Ems-6 represents subunits of the Cañizar Fm. and Eslida Fm. respectively.

Fig. 6. Description, interpretation and codes of the main and secondary fluvial and aeolian facies.

Fig. 7. Fluvial and aeolian architectural elements showing their codes, facies associations, hierarchy and vertical stacking patterns, and selected references.

Fig. 8. Pictures of the different described architectural elements: a) element GB in the Garraf Upper Conglomerates Unit (GUC), Catalan Ranges; b) element GM in the Prades Upper Conglomerates Unit (PUC), Catalan Ranges; c) SB and CH elements in the Cañizar Fm. (CS), Iberian Ranges; d) E1 element in Prades Lower Sandstone Unit (PLS), Catalan Ranges; e) E2 and E3 elements in Prades Lower Sandstone (PLS), Catalan Ranges; f) FF element in Figaró Sandstones and Mudstones (FSM), Catalan Ranges; f) GB element in the lowermost part of the "Buntsandstein" deposits of the Noves section, Pyrenean Ranges; h) E1 element in the lower Buntsandstein of the Noves section, Pyrenean Ranges. See figure 5 for the location of these units and sections.

Fig. 9. Sketches of 3D evolution of three selected stages of the Buntsandstein of the Iberian Ranges showing alluvial evolution and macroflora distribution (modified from Borruel-Abadía et al., 2014).

Fig. 10. Specimens of macroflora from the Eslida Fm. in the Iberian Ranges. a: *Pleuromeia sternbergii* (Münster) Corda ex Giebe, 1953; b: Sphenophytes, most likely *Equisetitesmougeotii* Brongniart 1828; c: *Pelourdea vogesiaca* (Schimper et Mogeot) Seaward 1917; d: *Albertia latifolia* Schimper et Mougeot 1944. Scale bar: 1 cm.

Fig. 11. A) Dispersed carbonate nodules are circled in the subsurface horizon of the Gat-A pedotype. Black arrows are pointing to small green root traces. B) Calcareous, rooted, and endurated yellow B horizons are irregularly truncated in the Pedotype Gat-B. C) Adventitious prop roots (marked in white) emanating from a main root in the Gat-C pedotype. White arrow is pointing to the top of another unmarked prop root pattern. D) Deep penetrating tap root with root apex (r) related to Gat-C paleosols. E) Drab-haloes of light green silt around root traces in the pedotype Gat-D.

Fig. 12. Synthesis of the main climate stages and their vertical alternating disposition during the Smithian to Pelsonian time – interval in the continental units (Buntsandstein) of the S. Iberian Ranges, E. Pyrenees and Catalan Ranges, and their relationship with fossil content. Sections (numbers 1 to 10) are located and named in figures 2 and 5.

Fig. 13. Early Triassic palaeogeographical reconstruction of Iberia and neighbour areas. Basins in Iberia were separated by elevated areas linked to the development of rift systems. Palaeolatitudes and sedimentary environments are partially based on Ziegler (1988), Dercourt et al. (1993), Mckie and Williams (2009), Bourquin et al. (2011) and Tyrrell et al. (2012).

Dear Editor,

In attached files (*Revision Notes*, *Revision changes marked* and *Clean version*) you will find the revised version of manuscript PALAEO8729 "*Climate changes during the Early-Middle Triassic transition in the E. Iberian Plate and its palaeogeographic significance in the western Tethys continental domain*", by Borrueal-Abadía et al.

First of all, we'd like to thank the detailed and interesting comments and recommendations sent by the reviewers and the Editor, as we consider all of them will improve the final version of this manuscript. All of them have been followed and carefully included in the final (clean) version and shown, one by one, in the "Revision, changed marked" item.

**Reviewer 1** sends a short list of interesting comments and recommendations, most of them (his points 5, 6, 7, 8 and 9) basically concentrated in two main topics that have needed a more detailed discussion. They are: a) the taphonomic biases of the paleobotanical record, and b) about what was driving the inferred climate changes (the case of the tectonics). This latter topic is also commented by reviewer 2. For answering these points, new paragraphs (as indicated in the Revision Notes) have been added.

Other aspects written by reviewer 1 (a total of 7 more, as the information published in some H. Bucher's papers, the influence of the Muschelkalk transgression, miss-spelled words....) are also of interest and answered here by the authors.

**Reviewer 2** concentrates his comments and recommendations in 4 main points. Points 1,2 and 4 basically recommends a reorganization in some paragraphs of the "Results - Discussion and Conclusion" chapters, as well as to reduce the length of the text eliminating some repetitions and by means of the own reorganization above suggested. These changes have needed more detailed (reorganization)modifications in the text, as is also shown in the "Revision, changed marked" item and therefore in the Clean version. The final result is clearly better than the original version. However the final length is not reduced as new paragraphs and references have been included, as suggested by both referees, for explaining other points.

In the "Revision, changed marked item", the added words/paragraphs suggested by the reviewer 1 are indicated in blue, and those suggested by reviewer 2 are indicated in green, while those eliminated are shown in red. All of these changes are also explained in the Revision Notes item.

Thank you again.

Kind regards,

José López-Gómez